

Accelerated Markov Chain Monte Carlo Algorithms on Discrete States

Bohan Zhou

*Department of Mathematics
University of California
Santa Barbara, CA 93106, USA.*

BHZHOU@UCSB.EDU

Shu Liu

*Department of Mathematics
Florida State University
Tallahassee, FL 32306, USA.*

SLIU11@FSU.EDU

Xinzhe Zuo

*Department of Mathematics
University of California
Los Angeles, CA 90095, USA.*

ZXZ@MATH.UCLA.EDU

Wuchen Li

*Department of Mathematics
University of South Carolina
Columbia, SC 29208, USA.*

WUCHEN@MAILBOX.SC.EDU

Abstract

We propose a class of discrete state sampling algorithms based on Nesterov's accelerated gradient method, which extends the classical Metropolis-Hastings (MH) algorithm. The evolution of the discrete states probability distribution governed by MH can be interpreted as a gradient descent direction of the Kullback–Leibler (KL) divergence, via a mobility function and a score function. Specifically, this gradient is defined on a probability simplex equipped with a discrete Wasserstein-2 metric with a mobility function. This motivates us to study a momentum-based acceleration framework using damped Hamiltonian flows on the simplex set, whose stationary distribution matches the discrete target distribution. Furthermore, we design an interacting particle system to approximate the proposed accelerated sampling dynamics. The extension of the algorithm with a general choice of potentials and mobilities is also discussed. In particular, we choose the accelerated gradient flow of the relative Fisher information, demonstrating the advantages of the algorithm in estimating discrete score functions without requiring the normalizing constant and keeping positive probabilities. Numerical examples, including sampling on a Gaussian mixture supported on lattices or a distribution on a hypercube, demonstrate the effectiveness of the proposed discrete-state sampling algorithm.

Keywords: Markov chain Monte Carlo methods; Metropolis-Hastings algorithms; Nesterov acceleration methods; Wasserstein metrics on graphs; discrete score functions; mobility functions.

AMS MSC: 65C05, 60J22, 82M31, 49Q22, 65K10

1 Introduction

Markov Chain Monte Carlo (MCMC) methods are algorithms to generate samples from a given probability distribution over a sampling space. A key advantage of the MCMC method is that it only requires knowledge of the target distribution up to a constant, making it well-suited for distributions with intractable normalizing constants—such as those arising in high-dimensional sampling spaces or in Bayesian posterior inference problems (Mengersen and Tweedie, 1996). This advantage has led to widespread applications of MCMC algorithms in various scientific domains, including Bayesian inference (Robert and Casella, 2004), computational physics and chemistry (e.g., simulating Ising models; see Metropolis et al. (1953); Hastings (1970); Landau and Binder (2015)), financial mathematics (e.g., risk modeling and option pricing; Jäckel (2002); Kou and Wang (2004); Jacquier et al. (2004)), and machine learning (e.g., energy-based models; Teh et al. (2004); Hinton et al. (2006); Salakhutdinov and Hinton (2009)).

In MCMC methods, the core idea is to construct a Markov chain with designed transition probabilities so that its stationary distribution is the target distribution π . Samples are then generated by running the chain for a sufficient number of steps. A well-known class of MCMC methods is the Langevin Monte Carlo (LMC) algorithm (Roberts and Tweedie, 1996a,b), which is based on the overdamped Langevin dynamics. LMC is designed to sample from a continuous sampling space by conducting gradient descent steps in the direction $\nabla \log \pi$, perturbed by an additive white noise. It is known that the evolution of the probability distribution p under LMC is a gradient flow of the Kullback-Leibler (KL) divergence on the space of probability distributions with the Wasserstein-2 metric (Villani, 2009). Here the Wasserstein-2 gradient of the KL divergence represents the score function $\nabla \log \frac{p}{\pi}$. Classical MCMC algorithms frequently encounter challenges such as slow convergence and poor mixing. This has motivated the demand for accelerated sampling algorithms. In recent decades, the Nesterov accelerated gradient (NAG) method (Nesterov, 1983; Su et al., 2016; Wibisono, 2018), a refinement of momentum-based optimization, has been shown to improve the convergence speed of gradient descent algorithms. This naturally raises the question of whether a Nesterov-type acceleration can be formulated for sampling, leveraging the Wasserstein gradient flow structure. This question has been investigated for continuous-space sampling from different approaches (Cheng et al., 2018; Taghvaei and Mehta, 2019; Ma et al., 2021; Wang and Li, 2022; Li et al., 2022; Zuo et al., 2025; Majee et al., 2025). See (Albritton et al., 2024; Cao et al., 2023; Brigati et al., 2025) and the references therein for convergence analysis under various norms. While there exists a rich literature on continuous-space sampling, many crucial sampling problems are defined over discrete spaces, as seen in statistical physics (Landau and Binder, 2015), combinatorics (Jerum and Sinclair, 1996), and discrete probabilistic graphical models (Jordan et al., 1999). A natural question arises:

How can we design a Nesterov accelerated sampling algorithm on discrete state spaces? What is the accelerated dynamics with discrete score functions?

In this paper, we mainly focus on sampling π on a finite *discrete* space $V = \{1, 2, \dots, n\}$. The Metropolis-Hastings (MH) algorithm (Metropolis et al., 1953; Hastings, 1970) serves as a foundational framework for sampling on discrete space. Given a candidate kernel (q_{ij}) , leveraging the acceptance ratio, the MH algorithm designs a *time-homogeneous* Markov

chain, with a transition rate matrix Q (Q_{ij} depends on (q_{ij})) that satisfies the *detailed-balance* condition $\pi_j Q_{ji} = \pi_i Q_{ij}$.

	Discrete-time	Continuous-time
MC	$\mathbb{P}(X^{(k+1)} = j \mid X^{(k)} = i) = P_{ij}$	$\mathbb{P}(X(t+h) = j \mid X(t) = i) \approx \delta_{ij} + Q_{ij}h$
FM	$p^{(k+1)} = p^{(k)}P$ in (4)	$\dot{p}(t) = pQ$ in (3)
GF	$p^{(k+1)} = p^{(k)}(I_n + Q\Delta t)$ in (4)	$\dot{p}(t) = -\nabla_p D_\phi(p\ \pi)\mathbb{K}(p)$ in (10)
HF	$p^{(k+1)} = p^{(k)}(I_n + \bar{Q}_\psi^r \Delta t)$ in (23), (24)	(1) is an instance of general framework (19)

Table 1: The conceptual flow in this work. “MC”, “FM”, “GF”, “HF” are abbreviations for Markov chain, forward master equation, gradient flow and Hamiltonian flow, respectively. We start with the Markov chain and end up with the damped Hamiltonian dynamics originated from Nesterov’s accelerated gradient method.

Analogous to the LMC algorithm on the continuous state space, which can be regarded as a gradient flow on the probability space, recent work (Maas, 2011; Erbar and Maas, 2012; Karatzas et al., 2021) has shown that the reversible Markov chain described in the forward master equation can be interpreted as the gradient flow of the KL divergence with respect to the discrete Wasserstein-2 metric, induced from a mobility function. The associated discrete Wasserstein-2 metric $\mathbb{K}(p)$ allows us to study the MCMC method as a first-order optimization algorithm on the probability simplex.

In this paper, we propose a momentum-based acceleration framework for discrete sampling. Our work is inspired by the interplay between the Wasserstein gradient flow structure of the MH algorithm and the NAG method. The key ingredients of our approach are summarized in Table 1. In particular, we consider a *damped Hamiltonian flow*, driven by the relative Fisher information:

$$\mathbb{I}(p\|\pi) = \frac{1}{4} \sum_{i,j=1}^n \pi_i Q_{ij} \theta_{ij}(p) \left(\log \frac{p_i}{\pi_i} - \log \frac{p_j}{\pi_j} \right)^2.$$

The dynamics evolve according to

$$\begin{cases} \frac{dp_i(t)}{dt} + \sum_{j \neq i} \pi_i Q_{ij} \theta_{ij}(p(t)) (\psi_j(t) - \psi_i(t)) = 0, \\ \frac{d\psi_i(t)}{dt} + \gamma(t) \psi_i(t) + \frac{1}{2} \sum_{j \neq i} \pi_i Q_{ij} \frac{\partial \theta_{ij}(p(t))}{\partial p_i} (\psi_i(t) - \psi_j(t))^2 + \frac{\partial \mathbb{I}(p(t)\|\pi)}{\partial p_i} = 0. \end{cases} \quad (1)$$

The first equation is a discrete-state continuity equation that describes the evolution of the probability function p . The second equation is a discrete Hamilton–Jacobi equation, which governs the dynamics of the momentum variable ψ , incorporating both dissipative effects

through the term $\gamma(t)\psi_i$ and information-theoretic feedback via $\frac{\partial \mathcal{I}(p||\pi)}{\partial p_i}$. Here, $\gamma(t)$ is a user-specified damping parameter. $(\theta_{ij}(p(t)))$ is a mobility weight matrix that may depend on $p(t)$. A particularly important choice is the *logarithmic mean* or *KL divergence mean*, given by

$$\theta_{ij}(p) = \frac{\frac{p_i}{\pi_i} - \frac{p_j}{\pi_j}}{\log \frac{p_i}{\pi_i} - \log \frac{p_j}{\pi_j}} = \frac{p_i}{\pi_i} \cdot \frac{1 - \frac{\pi_i p_j}{\pi_j p_i}}{\log \left(\frac{\pi_j p_i}{\pi_i p_j} \right)}. \quad (2)$$

The proposed accelerated MCMC (aMCMC) dynamics in (1) can be shown to guarantee the non-increasing behavior of its associated Hamiltonian function on a simplex set, defined as $\mathcal{H}(p, \psi) = \frac{1}{2}\psi\mathbb{K}(p)\psi^\top + \mathcal{I}(p||\pi)$, and the strict positivity of $p(t)$. For numerical implementation, we employ a staggered scheme to discretize (1) in time. Additionally, an interacting particle system on discrete states is introduced, with transition rates derived from a positive-negative decomposition of the gradient term $\psi_j - \psi_i$. We refer the reader to Section 5 for a detailed discussion of the algorithmic design.

Numerical experiments presented in Section 6 demonstrate that both the discrete time scheme and the particle swarm sampling-type algorithm achieve faster convergence to the target distribution π in ℓ^2 norm, compared with the MH method implemented in multi-chains for both fixed total number of iterations and fixed wall-clock times. Notably, the incorporation of score functions in the aMCMC algorithm yields a higher empirical accuracy, achieving an error of order $\mathcal{O}(\frac{1}{M})$, where M denotes the number of swarm particles. This marks a substantial improvement over the $\mathcal{O}(\frac{1}{\sqrt{M}})$ accuracy of the MH algorithm.

This paper is organized as follows: Section 2.1 reviews the classical MCMC with the MH update. Section 2.2 revisits the gradient flow formulation of the forward master equation, while Section 2.3 discusses gradient and accelerated flows in Euclidean space \mathbb{R}^d . Building on both perspectives, we introduce a class of aMCMC sampling algorithms on discrete-state spaces in Section 3, with particular instances listed in Table 2. The properties of proposed dynamics are discussed in Section 4. Section 5 describes the numerical scheme and some practical techniques including initialization and restart. Section 6 presents our numerical results. Lastly, we discuss our current limitations and future work in Section 7.

Methods	$\theta(\frac{p_i}{\pi_i}, \frac{p_j}{\pi_j})$	potential $\mathcal{U}(p)$	w/o Z	strict positivity
Chi-squared	1	$\frac{1}{2} \sum_{i=1}^n \frac{(p_i - \pi_i)^2}{\pi_i}$	No	No
KL	log-mean (2)	$\sum_{i=1}^n p_i \log \frac{p_i}{\pi_i}$	Yes	No
log-Fisher	log-mean (2)	$\frac{1}{4} \sum_{i,j=1}^n \omega_{ij} (\log \frac{\pi_j p_i}{\pi_i p_j}) (\frac{p_i}{\pi_i} - \frac{p_j}{\pi_j})$	Yes	Yes
con-Fisher	θ_{ij}	$\frac{1}{4} \sum_{i,j=1}^n \omega_{ij} \theta_{ij} (\log \frac{\pi_j p_i}{\pi_i p_j})^2$	Yes	Yes

Table 2: Examples of aMCMC dynamics. The 2nd column is the mobility weight matrix $(\theta_{ij}(p))$. The 3rd column is the potential function $\mathcal{U}(p)$. The 4th column is referred to if this method requires to know the normalizing constant Z of the target probability in prior. The 5th column is referred to if this method can ensure p to stay strictly positive.

Notations

The probability simplex $\mathbb{P}(V)$ supported on $V = \{1, 2, \dots, n\}$ is defined as

$$\mathbb{P}(V) = \left\{ p = [p_1, \dots, p_n] \in \mathbb{R}^n \mid p_i \geq 0 \text{ for any } i, \text{ and } \sum_{i=1}^n p_i = 1 \right\}.$$

We adopt the convention that vectors are represented as row vectors. Denote $T_p\mathbb{P}(V)$ as the tangent space of \mathbb{P} at p , then $T_p\mathbb{P}(V) = \{v = [v_1, \dots, v_n] \in \mathbb{R}^n \mid v_1 + \dots + v_n = 0\}$. The target probability is denoted by $\pi = [\pi_1, \dots, \pi_n]$, typically used as the stationary probability of the proposed dynamics governing the state variables $p(t) = [p_1(t), \dots, p_n(t)]$. For simplicity, we assume that π is strictly positive ($\pi_i > 0$ for all i). The transition probability matrix is denoted by $P = (P_{ij})$, where $P_{ij} = \mathbb{P}(X^{(k+1)} = j \mid X^{(k)} = i)$ represents the probability of transitioning from node i to node j . We adopt the row-sum-one convention, meaning $\sum_{j=1}^n P_{ij} = 1$ for each i . Additionally, we define the associated transition rate matrix as $Q = (Q_{ij})$, where $Q_{ij} \geq 0$ for non-diagonal entries, and $\sum_{j=1}^n Q_{ij} = 0$ for each i . Consequently, $Q_{ii} = -\sum_{j \neq i} Q_{ij}$. Let \bar{A}^r denote the row-sum-zero projection of any matrix

$$A \text{ such that } \begin{cases} \bar{A}_{ij}^r = A_{ij}, & \text{for } i \neq j; \\ \bar{A}_{ii}^r = -\sum_{j \neq i} A_{ij}. \end{cases} \quad \text{Thus for any transition rate matrix } Q, \bar{Q}^r = Q. \text{ We}$$

occasionally use the notation \bar{Q}^r in place of Q to highlight that Q is a row-sum-zero matrix. The stationary probability function π can be defined to satisfy that either $\pi P = \pi$ or $\pi Q = 0$.

Given a Q -matrix, it induces a directed weighted graph $G = (V, E, \omega)$ by: 1) $e_{ij} \in E$ if $Q_{ij} \neq 0$; 2) $\omega_{ij} = \pi_i Q_{ij}$. Under this choice, ω is row-sum-zero as well. Furthermore, if Q -matrix is reversible w.r.t its stationary probability π , i.e, $\pi_i Q_{ij} = \pi_j Q_{ji}$, then we say the associated Markov chain is *reversible* and we obtain an undirected graph G and a symmetric matrix ω .

The identity matrix in $\mathbb{R}^{n \times n}$ is denoted by I_n . A row vector of size n (a matrix of size $m \times n$) whose entries are ones is denoted by $\mathbb{1}_n$ ($\mathbb{1}_{m \times n}$, respectively). Similarly, $0_{n \times n}$ denotes the $n \times n$ zero matrix. $\mathbb{R}_+, \mathbb{R}_{\geq 0}$ are positive and nonnegative real numbers respectively. The orthogonal complement of the span $\{\mathbb{1}_n\}$ is $\mathbb{1}_n^\perp = \{v \in \mathbb{R}^n \mid \mathbb{1}_n \cdot v = 0\}$. For any square matrix $A \in \mathbb{R}^{n \times n}$, we denote $\text{Ker}(A) = \{x = [x_1, \dots, x_n] \mid xA = 0\}$.

2 Preliminaries

2.1 Metropolis-Hastings as the Forward Master Equation

Consider a *continuous-time reversible* Markov chain on a finite state space V . Let Q be a transition-rate matrix of the Markov chain, and $p(0) = [p_1(0), \dots, p_n(0)]$ be a probability function on V . The evolution dynamics of the probability function $p(t)$ with an initial data $p(0)$ is described by the forward master equation:

$$\frac{d}{dt} p_i = \sum_{j=1}^n p_j Q_{ji} - \sum_{j \neq i} p_j Q_{ij}, \quad (3)$$

whose stationary probability function is denoted by $\pi = [\pi_1, \dots, \pi_n]$. The forward master equation can be represented in a matrix form as $\frac{d}{dt} p = pQ$, by using $Q_{ii} = -\sum_{j \neq i} Q_{ij}$. From

the fundamental theorem of Markov chains, there is a unique, strictly positive stationary distribution π if we further assume the Markov chain is ergodic.

One can discretize (3) using the forward difference scheme. Given a step size $\Delta t > 0$, the discrete-time update satisfies

$$p^{(k+1)} = p^{(k)}P, \quad P = I_n + Q\Delta t \in \mathbb{R}^{n \times n}, \quad (4)$$

where I_n is the identity matrix. When Δt is chosen sufficiently small, the matrix P is a valid transition probability matrix so that (4) is a discrete-time jump process.

In a sampling algorithm, Q must be designed to ensure that the probability distribution $p(t)$ converge to the given target distribution π . The Metropolis-Hastings algorithm proposes a generic way to construct a *discrete-time* Markov-chain on V , that is ergodic (i.e., irreducible and aperiodic) and stationary with respect to π . Given a user-specified conditional density $q_{ij} = \mathbb{P}(Y = j \mid X = i)$, also known as the *candidate kernel*, MH designs an acceptance-rejection matrix:

$$A_{ij} := A(X = i, Y = j) = \begin{cases} \min \left\{ \frac{\pi_j q_{ji}}{\pi_i q_{ij}}, 1 \right\}, & \pi_i q_{ij} > 0; \\ 1, & \pi_i q_{ij} = 0. \end{cases}$$

A key advantage is that the acceptance-rejection probability depends on the ratio of $\frac{\pi_j}{\pi_i}$, eliminating the need to know the normalizing constant for π (Ottobre, 2016). In this work we use the standard random walk MH scheme for (q_{ij}) as a benchmark for comparisons. The Metropolis-Hastings algorithm is presented in Algorithm 1.

Algorithm 1: Metropolis-Hastings algorithms

Input : Initial data $X^{(0)}$, target distribution π , candidate kernel q , total iterations N .
Output: The Markov chain $(X^{(i)})_{i=1}^N$.

- 1 **for** $i \leftarrow 0$ **to** N **do**
- 2 Propose a candidate $Y^{(i)} \sim q(y \mid X^{(i)})$;
- 3 Generate $u^{(i)} \sim \text{uniform}[0, 1]$;
- 4 Set $X^{(i+1)} = Y^{(i)}$ if $u \leq A(X^{(i)}, Y^{(i)})$; otherwise $X^{(i+1)} = X^{(i)}$.
- 5 **end**

The acceptance-rejection matrix induces a transition rate matrix for (3), satisfying the detailed balance condition:

$$Q_{ij}^{\text{MH}} := q_{ij}A_{ij} = \min \left\{ \frac{\pi_j}{\pi_i} q_{ji}, q_{ij} \right\}. \quad (5)$$

In summary, the MH algorithm yields a reversible and ergodic Markov chain on a discrete state space V . Starting from an arbitrary initial distribution $p(0)$, the time evolution of the probability distribution $p(t)$ under the MH dynamics is governed by (3), alternatively, the jump process $p^{(k)}$ arising from MH can be described by (4), specifically using the transition rate matrix Q^{MH} .

One advantage of Q^{MH} is its time-homogeneity, which simplifies implementation in numerical experiments. Additionally, Q^{MH} is dependent of the normalizing constant Z for π . However, it may suffer from *pseudo-convergence* in multimodal distribution (see Geyer, 2011, Chapter 1.11.2). In practice, MH sampling can proceed either by running a single long chain or by averaging over multiple shorter chains.

Schnakenberg (1976) shows that given any transition rate probability matrix Q and the target distribution π , there is a weighted directed graph representation $G = (V, E, \omega)$ of the forward master equation, where weight matrix ω is given by $(\omega_{ij}) = (\pi_i Q_{ij})$. In the specific case where $Q = Q^{\text{MH}}$, the detailed balance condition implies that $\omega_{ij} = \omega_{ji}$, rendering G an undirected graph that permits self-loops but excludes multiple edges. Our primary focus in this work is sampling on the corresponding undirected graph $G = (V, E, \omega)$ with $Q = Q^{\text{MH}}$.

2.2 Reversible Markov Chain as a Wasserstein Gradient Flow

A series of seminal works (Maas, 2011; Erbar and Maas, 2012; Mielke, 2013; Karatzas et al., 2021) interpret the reversible Markov chain on a discrete state space as the “gradient flow” of the entropy functional over the probability manifold $\mathbb{P}(V)$, by introducing a graphical version of the Wasserstein metric, and exploiting the geodesic convexity of the entropy w.r.t. this metric. In this subsection, we provide a brief review with a focus on the Wasserstein gradient flow and postpone the discussion on convexity to Section 4.4 and Appendix D.

We refer interested readers to (Otto, 2001; Ambrosio et al., 2008; Villani, 2009) for Wasserstein gradient flows (WGF) on continuous state spaces; and to (Maas, 2011; Chow et al., 2012) on discrete state spaces. In these studies, the probability manifold is endowed with a Riemannian metric known as the Wasserstein metric. The so-called *Otto calculus* (Otto, 2001) is then used to introduce a gradient flow interpretation on the probability manifold for a family of evolution equations.

We first recall approaches in (Mielke, 2013; Gao et al., 2024) to treat the gradient structure w.r.t. the Riemannian metric. In optimization, it is equivalent to apply a preconditioning matrix—commonly known as *Onsager’s response* matrix \mathbb{K} —onto the flat gradient. Given a convex function $f : \mathbb{R}_{\geq 0} \mapsto \mathbb{R}$ that satisfies $f(1) = 0$, $f(0) = \lim_{x \rightarrow 0^+} f(x)$, and $f''(x) > 0$ for $x > 0$, we define the f -divergence on $\mathbb{P}(V)$ as

$$D_f(p||\pi) = \sum_{i=1}^n f\left(\frac{p_i}{\pi_i}\right) \pi_i. \quad (6)$$

By Jensen’s inequality, $D_f(p||\pi) \geq f(1) = 0$. A common choice of f is $f(x) = x \log x$. This yields the Kullback–Leibler divergence $D_{\text{KL}}(p||\pi) = \sum_{i=1}^n p_i \log\left(\frac{p_i}{\pi_i}\right)$.

Due to the detailed balance $\omega_{ij} = \pi_i Q_{ij} = \pi_j Q_{ji} = \omega_{ji}$, we can rewrite the forward master equation (3) as

$$\begin{aligned} \frac{d}{dt} p_i &= \sum_{j \neq i} p_j Q_{ji} - p_i Q_{ij} = \sum_{j \neq i} \frac{p_j}{\pi_j} \pi_j Q_{ji} - \frac{p_i}{\pi_i} \pi_i Q_{ij} = \sum_{j \neq i} \omega_{ij} \left(\frac{p_j}{\pi_j} - \frac{p_i}{\pi_i} \right) \\ &= \sum_{j \neq i} \omega_{ij} \theta_{ij}(p) \left(f'\left(\frac{p_j}{\pi_j}\right) - f'\left(\frac{p_i}{\pi_i}\right) \right), \end{aligned} \quad (7)$$

where we introduce a mobility function $\theta(x, y)$ (also known as an activation function, see Gao et al. (2024)) as

$$\theta(x, y) = \begin{cases} \frac{x - y}{f'(x) - f'(y)} & x \neq y; \\ \frac{1}{f''(x)} & x = y, \end{cases} \quad (8)$$

and use the abbreviation $\theta_{ij}(p) = \theta(\frac{p_i}{\pi_i}, \frac{p_j}{\pi_j})$.

Now we define the Onsager's response matrix $\mathbb{K}(p)$ as

$$\mathbb{K}_{ij}(p) = -\omega_{ij}\theta_{ij}(p) \quad \text{and} \quad \mathbb{K}_{ii}(p) = -\sum_{j \neq i} \mathbb{K}_{ij}(p). \quad (9)$$

$\mathbb{K}(p)$ is row-sum-zero and symmetric. One can verify that $\mathbb{K}(p)$ is positive semi-definite with $\text{Ker}(\mathbb{K}(p)) = \text{span}(\mathbb{1}_n)$. We refer the readers to Appendix A for detailed discussion. In fact, $\mathbb{K}(p)$ is the graph Laplacian of a weighted undirected graph with a weight matrix $(\omega_{ij}\theta_{ij})$.

Since $\partial_{p_j} D_f(p|\pi) = f'(\frac{p_j}{\pi_j})$, (7) can be rewritten as $\frac{d}{dt} p_i = -\sum_{j=1}^n \mathbb{K}_{ij}(p) \partial_{p_j} D(p|\pi)$.

Denote by $\nabla_p D(p|\pi) := [\partial_{p_1} D(p|\pi), \dots, \partial_{p_n} D(p|\pi)]$, we have

$$\frac{d}{dt} p = -\nabla_p D(p|\pi) \mathbb{K}(p), \quad \text{or equivalently} \quad \frac{d}{dt} p \mathbb{K}^\dagger(p) = -\nabla_p D(p|\pi), \quad (10)$$

where $\mathbb{K}^\dagger(p)$ is the Moore-Penrose inverse of $\mathbb{K}(p)$. Thus (10) is employed with a preconditioning matrix $\mathbb{K}(p)$ on the gradient $\nabla_p D(p|\pi)$ from the view of optimization.

Consider a curve $p(t)$ on $\mathbb{P}(V)$ parametrized by a time variable t , we denote its tangent vector by $\dot{p}(t)$. Define the *graphical Wasserstein* metric tensor $g_W(\cdot, \cdot)$ as

$$g_W(\dot{p}(t), \dot{p}(t)) = \frac{1}{2} \sum_{i=1}^n \sum_{j \neq i} \omega_{ij} \theta_{ij}(p(t)) (\psi_i(t) - \psi_j(t))^2 = \psi(t) \mathbb{K}(p(t)) (\psi(t))^\top, \quad (11)$$

where $\psi(t) = [\psi_1(t), \dots, \psi_n(t)]$ denotes the momentum (cotangent) vector associated with the tangent vector $\dot{p}(t)$. We have the following graphical continuity equation:

$$\dot{p}_i(t) + \sum_{j \neq i} \omega_{ij} \theta_{ij}(p(t)) (\psi_j(t) - \psi_i(t)) = 0, \quad \text{that is,} \quad \dot{p} - \psi \mathbb{K}(p) = 0. \quad (12)$$

Thus the inner product (11) is expressed as

$$g_W(\dot{p}(t), \dot{p}(t)) = \dot{p}(t) \mathbb{K}^\dagger(p) \dot{p}(t)^\top. \quad (13)$$

One can interpret $g_W(\cdot, \cdot)$ as a Riemannian metric on $\mathbb{P}(V)$ with a metric tensor $\mathbb{K}^\dagger(p)$

It is worth noting that $\text{Ker}(\mathbb{K}(p)^\dagger) = \text{Ker}(\mathbb{K}(p)) = \text{span}(\mathbb{1}_n)$. One can verify that $\mathbb{K}(p)$ is positive definite on $\mathbb{1}_n^\perp$, and so is $\mathbb{K}(p)^\dagger$. Since the tangent space $T_p \mathbb{P}(V)$ at p corresponds to $\mathbb{1}_n^\perp$, $\mathbb{K}(p)^\dagger$ is positive definite on $T_p \mathbb{P}(V)$ for all $p \in \mathbb{P}(V)$. Consequently, one can treat $g_W(\cdot, \cdot)$ as a Riemannian metric on $\mathbb{P}(V)$. Such a metric also determines the geodesic and

the corresponding distance function on $(\mathbb{P}(V), g_W)$. One can introduce the *kinetic energy* on the graph from the Riemannian metric by

$$\frac{1}{2}g_W(\dot{p}(t), \dot{p}(t)) = \frac{1}{2}\psi(t)\mathbb{K}(p(t))\psi(t)^\top = \frac{1}{4}\sum_{i=1}^n\sum_{j\neq i}^n\omega_{ij}\theta_{ij}(p(t))(\psi_i(t) - \psi_j(t))^2.$$

Furthermore, analogous to the Benamou-Brenier theorem (Benamou and Brenier, 2000) in continuous space, the graphical version of the Wasserstein metric between two probabilities p_0 and p_1 on the probability manifold $\mathbb{P}(V)$ is defined as follows:

$$W_2^2(p_0, p_1) = \inf_{p, \psi} \left\{ \frac{1}{2} \int_0^1 \sum_{i=1}^n \sum_{j\neq i}^n \omega_{ij} \theta_{ij}(p(t)) (\psi_i(t) - \psi_j(t))^2 dt \right\}, \quad (14)$$

where the infimum is taken over all sufficiently regular curves $p : [0, 1] \mapsto \mathbb{P}(V)$ and $\psi : [0, 1] \mapsto \mathbb{R}^n$ that satisfy the graphical continuity equation (12) with boundary conditions $p(0) = p_0, p(1) = p_1$. And the minimizer $p(t)$ is the geodesic from p_0 to p_1 on the Riemannian manifold $(\mathbb{P}(V), g_W)$. Consequently, (10) is the *Wasserstein gradient flow* of $D_f(\cdot \|\pi)$ on $(\mathbb{P}(V), g_W)$:

$$\frac{dp}{dt} = -\text{grad}D_f(p \|\pi) = -\nabla_p D_f(p \|\pi) \mathbb{K}(p).$$

The detailed derivation for the Wasserstein gradient $\text{grad}D_f(p \|\pi)$ can be founded in Appendix A.

2.3 Gradient Flow and Accelerated Flow in \mathbb{R}^n

In this subsection, we review some basic concepts and results from classical optimization in the Euclidean space \mathbb{R}^d . This perspective will help clarify how an accelerated framework can emerge naturally from gradient flows.

Let $U : \mathbb{R}^d \rightarrow \mathbb{R}$ be a \mathcal{C}^1 convex function. The classical gradient descent method for finding the global minimum of $U(x)$ consists of iteratively moving in the negative gradient direction at a small step size Δt

$$x^{(k+1)} = x^{(k)} - \Delta t \nabla U(x^{(k)}).$$

Convergence of the gradient descent algorithm can be guaranteed when $U(x)$ is L -smooth and $0 < \Delta t < 1/L$. Then one has $U(x^{(k)}) - U(x^*) = \mathcal{O}(k^{-1})$, where $U(x^*)$ is the minimum value. If $U(x)$ is further assumed to be λ -strongly convex, then with the choice of $\Delta t = 1/L$, one has linear convergence: $U(x^{(k)}) - U(x^*) = \mathcal{O}((1 - \lambda/L)^k)$.

The gradient flow can be viewed as the limit of the gradient descent as $\Delta t \rightarrow 0$. We consider instead the continuous trajectory $x(t)$ which follows the first-order ODE:

$$\dot{x}(t) = -\nabla U(x(t))$$

for $t > 0$ with the initial condition $x(0) = x_0$. It is well known that the convergence rate of gradient flow is $\mathcal{O}(t^{-1})$ for convex functions. If f is λ -strongly convex for some $\lambda > 0$, then gradient flow converges at a rate of $\mathcal{O}(e^{-\lambda t})$.

The seminal paper Nesterov (1983) proposed the following iteration scheme to minimize a convex function $U(x)$ with some initial guess $x_0 = y_0$:

$$\begin{cases} x^{(k)} = y^{(k-1)} - \Delta t \nabla U(y^{(k-1)}), \\ y^{(k)} = x^{(k)} + \frac{k-1}{k+2}(x^{(k)} - x^{(k-1)}). \end{cases} \quad (15)$$

With the choice of $0 < \Delta t \leq 1/L$, this scheme can be shown to converge at a much faster rate than the gradient descent. Specifically, $U(x^{(k)}) - U(x^*) = \mathcal{O}(\frac{1}{\Delta t k^2})$. As a result, Nesterov's method is also referred as the *accelerated gradient* method.

For λ -strongly convex and L -smooth functions, Nesterov's iterations are

$$\begin{cases} x^{(k)} = y^{(k-1)} - \Delta t \nabla U(y^{(k-1)}), \\ y^{(k)} = x^{(k)} + \frac{\sqrt{\kappa} - 1}{\sqrt{\kappa} + 1}(x^{(k)} - x^{(k-1)}). \end{cases} \quad (16)$$

Here $\kappa = \frac{\lambda}{L}$ is the condition number. With the choice of $\Delta t = 1/L$, one can show that $U(x^{(k)}) - U(x^*) = \mathcal{O}(e^{-k/\sqrt{\kappa}})$.

In contrast to the gradient flow, the continuous version of the Nesterov acceleration is a second order ODE, first proposed and studied by Su et al. (2016):

$$\ddot{x} + \gamma(t)\dot{x} + \nabla U(x) = 0, \quad (17)$$

with initial condition $x(0) = x_0$, $\dot{x}(0) = 0$. Here $\gamma(t)$ is a user-specified damping parameter that can be time-homogeneous or time-inhomogeneous. When $U(x)$ is convex, the original Nesterov's iterations (15) corresponds to the choice $\gamma(t) = \frac{3}{t}$. When $U(x)$ is further assumed to be λ -strongly convex, (16) corresponds to the choice $\gamma(t) = 2\sqrt{\lambda}$.

An important observation by Maddison et al. (2018) is that the second-order ODE (17) can be formulated as

$$\begin{bmatrix} \dot{x} \\ \dot{v} \end{bmatrix} + \begin{bmatrix} 0 \\ \gamma(t)v \end{bmatrix} - \begin{bmatrix} 0 & I \\ -I & 0 \end{bmatrix} \begin{bmatrix} \partial_x \mathcal{H}(x, v) \\ \partial_v \mathcal{H}(x, v) \end{bmatrix} = 0, \quad (18)$$

where x is the state variable and v is the momentum variable. $\mathcal{H}(x, v) \triangleq \|v\|^2/2 + U(x)$ is the Hamiltonian function. This formulation lifts the second-order ODE to a system of ODEs, and shows that the accelerated gradient flow can be viewed as a damped Hamiltonian flow.

Zhang and Sra (2018) proposed the Riemannian version of Nesterov's method for geodesically smooth and strongly convex problems. Borrowing ideas from Su et al. (2016), Alimisis et al. (2020) generalized Nesterov's ODE to a Riemannian manifold (\mathcal{M}, g) :

$$\ddot{X} + \gamma(t)\dot{X} + \text{grad}_{\mathcal{M}}U(X) = 0,$$

where $X \in \mathcal{M}$ and $\text{grad}_{\mathcal{M}}U(X)$ is the Riemannian gradient of U at X . In particular, when U is geodesically convex, Alimisis et al. (2020) proved an $\mathcal{O}(t^{-2})$ convergence rate, matching the convergence rate in Euclidean space. The choice of the damping parameter $\gamma(t)$ also depends on the lower bound of the sectional curvature of the manifold \mathcal{M} .

3 Nesterov Acceleration on Probability Manifolds

Given a target probability π and an irreducible Q -matrix that is reversible w.r.t π , they induce a graph $G = (V, E, \omega)$ with a weight matrix $(\omega_{ij}) = (\pi_i Q_{ij})$. For the probability manifold $\mathbb{P}(V)$, selecting an eligible activation function θ_{ij} in the form of (8) determines the Onsager's response matrix $\mathbb{K}(p)$ via (9), which induces a Riemannian metric on $\mathbb{P}(V)$. Within this framework, we construct a damped Hamiltonian dynamics for a pair of state and momentum variables $(p(t), \psi(t))$,

$$\begin{bmatrix} \dot{p}(t) \\ \dot{\psi}(t) \end{bmatrix} = \begin{bmatrix} 0 \\ -\gamma(t)\psi(t) \end{bmatrix} + \begin{bmatrix} 0 & I \\ -I & 0 \end{bmatrix} \begin{bmatrix} \partial_p \mathcal{H}(p(t), \psi(t)) \\ \partial_\psi \mathcal{H}(p(t), \psi(t)) \end{bmatrix}, \quad (19)$$

where $\gamma(t)$ is a user-specified positive damping parameter. (19) is a variant of (18), inspired by previous works on the Euclidean space (Su et al., 2016; Maddison et al., 2018) and on the probability manifold (Wang and Li, 2022; Chen et al., 2025).

The Hamiltonian $\mathcal{H}(p, \psi)$ is defined as follows

$$\mathcal{H}(p, \psi) = \frac{1}{2} \psi \mathbb{K}(p) \psi^\top + \mathcal{U}(p) = \frac{1}{4} \sum_{i=1}^n \sum_{j \neq i} \omega_{ij} \theta_{ij}(p) (\psi_i - \psi_j)^2 + \mathcal{U}(p), \quad (20)$$

where $\mathcal{U} : \mathbb{P}(V) \rightarrow \mathbb{R}$ is a function, whose unique critical point is the target probability π . The first term in (20) can be interpreted as the graphical analogue of kinetic energy. The second term can be viewed as the potential energy in the classical Hamiltonian system.

We expand the matrix form (19) into the template ODEs by plugging (20),

$$\begin{cases} \frac{dp_i}{dt} + \sum_{j \neq i} \omega_{ij} \theta_{ij}(p) (\psi_j - \psi_i) = 0, & (21a) \\ \frac{d\psi_i}{dt} + \gamma(t)\psi_i + \frac{1}{2} \sum_{j \neq i} \omega_{ij} \frac{\partial \theta_{ij}(p)}{\partial p_i} (\psi_i - \psi_j)^2 + \frac{\partial \mathcal{U}(p)}{\partial p_i} = 0, & (21b) \end{cases}$$

where (21a) can be written compactly as $\frac{d}{dt} p = \psi \mathbb{K}(p)$ while the second equation is in general nonlinear. Users may specify the weight matrix ω , the activation function $\theta(p)$, the potential $\mathcal{U}(p)$ and the damping parameter $\gamma(t)$ in this system. We will discuss examples shown in Table 2 in the following subsections.

In general, (21) has these basic properties:

- $\mathcal{H}(p(t), \psi(t))$ is nonincreasing. Since

$$\begin{aligned} \frac{d\mathcal{H}(t)}{dt} &= \partial_p \mathcal{H} \cdot \frac{dp(t)}{dt} + \partial_\psi \mathcal{H} \cdot \frac{d\psi(t)}{dt} = \partial_p \mathcal{H} \cdot \psi + \partial_\psi \mathcal{H} \cdot (-\gamma(t)\psi(t) - \partial_p \mathcal{H}) \\ &= -\gamma(t) \partial_\psi \mathcal{H} \cdot \psi(t) = -\gamma(t) (\psi(t) \mathbb{K}(p)) \cdot \psi(t) \leq 0. \end{aligned} \quad (22)$$

- $p(t) \in \mathbb{P}(V)$ is provided with $p(0) \in \mathbb{P}(V)$. Since

$$\dot{p}(t) \mathbb{1}_n^\top = \partial_\psi \mathcal{H} \mathbb{1}_n^\top = \psi(t) \mathbb{K}(p(t)) \mathbb{1}_n^\top = 0.$$

- $p(t)$ driven by (21) must converge to π . From (21a), for any stationary point (p^*, ψ^*) to (21), it is necessary that $\psi_i^* = \psi_j^* = c$ for some constant c . Consequently, $\frac{\partial \mathcal{U}(p^*)}{\partial p_i} = 0$ from (21b). Note that π is the unique critical point to $\mathcal{U}(p)$.

To construct a sampling algorithm (a “jump process” of particles on V), we rewrite (21a) in the form of the forward master equation

$$\frac{d}{dt}p = p\bar{Q}_\psi^r, \quad (23)$$

and discretize it in time to obtain the jump process. The derivation can be found in Appendix C. Here, the notation \bar{Q}_ψ^r is to resemble the Q -matrix used in Section 2.1 and is row-sum-zero, given by

$$\begin{bmatrix} -\sum_{j \neq 1} \frac{\omega_{1j}\theta_{1j}(p)(\psi_1 - \psi_j)_-}{p_1} & \frac{\omega_{12}\theta_{12}(p)(\psi_2 - \psi_1)_+}{p_1} & \dots & \frac{\omega_{1n}\theta_{1n}(p)(\psi_n - \psi_1)_+}{p_1} \\ \frac{\omega_{21}\theta_{21}(p)(\psi_1 - \psi_2)_+}{p_2} & -\sum_{j \neq 2} \frac{\omega_{2j}\theta_{2j}(p)(\psi_2 - \psi_j)_-}{p_2} & \dots & \frac{\omega_{2n}\theta_{2n}(p)(\psi_n - \psi_2)_+}{p_2} \\ \vdots & \dots & \ddots & \vdots \\ \frac{\omega_{n1}\theta_{n1}(p)(\psi_1 - \psi_n)_+}{p_n} & \frac{\omega_{n2}\theta_{n2}(p)(\psi_2 - \psi_n)_+}{p_n} & \dots & -\sum_{j \neq n} \frac{\omega_{nj}\theta_{nj}(p)(\psi_n - \psi_j)_-}{p_n} \end{bmatrix} \quad (24)$$

where $(\psi_i - \psi_j)_+ := \max\{\psi_i - \psi_j, 0\}$ and $(\psi_i - \psi_j)_- := -\min\{\psi_i - \psi_j, 0\}$. Notably, if $p_i(t) = 0$, then the i -th row is undefined. In order to use $P = I_n + \bar{Q}_\psi^r \Delta t$ as the transition probability matrix in the jump process, it is crucial to ensure the *strict positivity* of $p_i(t)$ for any i and any $t > 0$.

Remark 1 *The reformulation of our dynamics in terms of the forward master equation (23) enables a formal comparison with the MH method reviewed in Section 2.1. Using the same candidate kernel q_{ij} as in the acceptance-rejection matrix A_{ij} in (5) for the MH method, the corresponding acceptance-rejection matrix of our jump process takes the form*

$$(\bar{A}_\psi)_{ij} := \max \left\{ \frac{\omega_{ij}\theta_{ij}(p)(\psi_j - \psi_i)}{p_i q_{ij}}, 0 \right\} = \max \left\{ \frac{\pi_i \theta_{ij}(p)}{p_i} (\psi_j - \psi_i), 0 \right\} A_{ij}. \quad (25)$$

*It is also possible to derive an equivalent form of the forward master equation under a different Q -matrix, resulting in a different acceptance-rejection matrix, see one example for the **Chi-squared** method in Section 3.1. As noted in Le and Miclo (2026), which is motivated by considerations analogous to those underlying our dynamics in the setting of interacting particle systems (i.e., swarm dynamics), although (24) admits a Markovian interpretation, the resulting process is nonlinear in the sense that it interacts with its law. Consequently, it requires the simulation of multiple chains or, equivalently, the evolution of empirical distributions. By contrast, the Metropolis-Hastings algorithm presented in Algorithm 1 can run in a single long chain, even though it may suffer from poor initialization, have long burn-in time or show pseudo-convergence (Geyer, 2011). This limitation has motivated the development of the multiple-chain variants of MH algorithms; see, e.g., Gelman and Rubin (1992); Jasra et al. (2007); Craiu et al. (2009); Jacob et al. (2011); Calderhead (2014).*

In the following subsections, we present some examples of activation and potential functions. In this paper, we focus mainly on the activation function $\theta_{ij}(p) = \frac{\frac{p_i}{\pi_i} - \frac{p_j}{\pi_j}}{f'(\frac{p_i}{\pi_i}) - f'(\frac{p_j}{\pi_j})}$ motivated by Wasserstein gradient flows (10), and the corresponding potential $\mathcal{U}(p)$ either as f -divergences or relative Fisher information functions.

For the former potential by f -divergences, from the perspectives outlined in Section 2.2 and Section 2.3, the corresponding forward master equation (3) can be interpreted as the gradient flow of the f -divergence in the probability manifold equipped with the graphical Wasserstein metric (14). Consequently the damped Hamiltonian dynamics (19) driven with f -divergence as its potential, can be regarded as the Nesterov accelerated flow in the probability manifold. We also note that the Hamiltonian flow with the relative Fisher information function in the Wasserstein space has been studied for Schrödinger equations; see related motivations in (Nelson, 1966; von Renesse, 2012; Chow et al., 2019). In this paper, we design a damped Hamiltonian flow on the simplex set, which uses the relative Fisher information functional to maintain the strict positivity of the probability function.

We present the explicit form of (21) under the selected activation and potential functions in each subsequent subsections. The detailed derivations for Section 3.1 - Section 3.3 can be founded in Appendix C.

3.1 χ^2 Divergence and Uniform Activation

In this subsection, we select $\theta_{ij} = 1$ and χ^2 divergence $\mathcal{U}(p) = \frac{1}{2} \sum_{i=1}^n \frac{(p_i - \pi_i)^2}{\pi_i}$. It is clear that $\mathcal{U}(p) \geq 0$ and $\mathcal{U}(\pi) = 0$. Now (21) reads

$$\begin{cases} \frac{dp_i}{dt} = \psi_i \sum_{j \neq i} \omega_{ij} - \sum_{j \neq i} \psi_j \omega_{ji}, \\ \frac{d\psi_i}{dt} + \gamma(t)\psi_i + \frac{p_i}{\pi_i} - 1 = 0. \end{cases} \quad (26)$$

Denote by $[p, \psi] = [p_1, \dots, p_n, \psi_1, \dots, \psi_n]$, we rewrite (26) into a matrix equation:

$$\frac{d}{dt}[p, \psi] = [p, \psi]L + [0_{1 \times n}, \mathbb{1}_{1 \times n}],$$

where the matrix L is given by

$$L \triangleq \begin{bmatrix} 0_{n \times n} & -\text{diag}(\frac{1}{\pi}) \\ K & -\gamma(t)I_n \end{bmatrix}, \quad (27)$$

where $\text{diag}(\frac{1}{\pi})$ represents a diagonal matrix with diagonal entries $(\frac{1}{\pi_1}, \dots, \frac{1}{\pi_n})$. Choosing $\theta_{ij} = 1$ results in a constant matrix K , which corresponds to a flat metric of $\mathbb{P}(V)$. We will refer to this method as the **Chi-squared** method.

The vector form of (26) can be reformulated as the second-order ODE $\frac{d^2 p}{dt^2} + \gamma(t) \frac{dp}{dt} - pQ = 0$, which is the Telegrapher's equation (Archer, 2009). In coordinates, this equation reads

$$\frac{d^2 p_i}{dt^2} + \gamma(t) \frac{dp_i}{dt} - \sum_{j \neq i} (p_j Q_{ji} - p_i Q_{ij}) = 0. \quad (28)$$

Remark 2 From the time discretizations of the equation on the state variables (26) and of the above Telegrapher's equation (28), we obtain a non-Markovian process (a jump process for every two steps, i.e., from $p^{(k)}$ to $p^{(k+2)}$),

$$p_i^{(k+2)} = p_i^{(k)} + (\Delta t)^2 \sum_{j \neq i} \left[Q_{ji} + \frac{2 - \gamma(t)\Delta t}{\Delta t} \frac{\pi_j Q_{ji} (\psi_i^{(k)} - \psi_j^{(k)})_+}{p_j^{(k)}} \right] p_j^{(k)} \\ + (\Delta t)^2 \left[-Q_{ij} - \sum_{j \neq i} \frac{\pi_i Q_{ij} (\psi_i^{(k)} - \psi_j^{(k)})_-}{p_i^{(k)}} \right] p_i^{(k)},$$

see Appendix C for details. Thus the acceptance-rejection matrix can be formally defined as

$$(\bar{A}_\psi)_{ij} = \left(1 + \frac{2 - \gamma(t)\Delta t}{\Delta t} \frac{\pi_j}{p_j} (\psi_i - \psi_j)_+ \right) A_{ij}, \quad (29)$$

where $A_{ij} = \frac{Q_{ij}}{q_{ij}}$ is the acceptance-rejection matrix from MH from (5). Notably, (29) is not the special case of (25) after plugging $\theta_{ij} = 1$. The design of an optimal step size Δt for the corresponding new numerical scheme is left for future work.

3.2 KL Divergence and Logarithmic Mean

In this subsection, we choose the logarithmic mean $\theta_{ij}(p) = \frac{p_j - p_i}{\frac{p_j}{\pi_j} - \frac{p_i}{\pi_i}}$ in (2) and the *Kullback-Leibler* (KL) divergence $\mathcal{U}(p) = \sum_{i=1}^n p_i \log \frac{p_i}{\pi_i}$. It is clear that $\mathcal{U}(p) \geq 0$ and $\mathcal{U}(p) = 0$ if and only if $p = \pi$. Under these choices, (21) becomes

$$\begin{cases} \frac{dp_i}{dt} = \sum_{j \neq i} \pi_i Q_{ij} \frac{p_i - p_j}{\log \frac{\pi_j p_i}{\pi_i p_j}} (\psi_i - \psi_j), \\ \frac{d\psi_i}{dt} + \gamma(t)\psi_i + \log \frac{p_i}{\pi_i} + \frac{1}{2} \sum_{j \neq i} Q_{ij} \frac{\log \left(\frac{\pi_j p_i}{\pi_i p_j} \right) - 1 + \left(\frac{\pi_j p_i}{\pi_i p_j} \right)^{-1}}{\log^2 \left(\frac{\pi_j p_i}{\pi_i p_j} \right)} (\psi_i - \psi_j)^2 = 0. \end{cases} \quad (30)$$

We will refer this method as the KL method in subsequent sections. The choice of θ and $\mathcal{U}(p)$ in the KL method is natural, since it can be regarded as the Nesterov accelerated flow for the KL divergence in the probability manifold $(\mathbb{P}(V), g_W)$. However, the positivity of density $p(t)$ might not be preserved under the functional $\mathcal{U}(p) = \sum p_i \log \frac{p_i}{\pi_i}$. One has to select a careful numerical scheme in order to do the jump process proposed in the beginning of this section. Therefore we propose the relative Fisher information in the following subsections to tackle this issue.

3.3 The Relative Fisher Information and Logarithmic Mean

We still select the logarithmic mean while choose the potential energy $\mathcal{U}(p) = \mathbb{I}(p||\pi) = \frac{1}{4} \sum_{i=1}^n \sum_{j \neq i} \omega_{ij} (\log \frac{p_i}{\pi_i} - \log \frac{p_j}{\pi_j}) (\frac{p_i}{\pi_i} - \frac{p_j}{\pi_j})$ as the relative Fisher information $\mathbb{I}(p||\pi)$. Notably, $\mathbb{I}(p||\pi) \geq 0$, with equality if and only if $\frac{p_i}{\pi_i} = \frac{1}{Z}$ for all i . The following lemma shows that the relative Fisher information has a unique critical point.

Lemma 3 *Given a strictly positive target probability π and an irreducible transition-rate matrix Q , then $p > 0$ is a critical point of $I(p|\pi)$ in $\mathbb{P}(V)$, i.e., $\nabla_p I(p|\pi) = 0$, if and only if $p = \pi$.*

(21) takes the form

$$\begin{cases} \frac{dp_i}{dt} = \sum_{j \neq i} \pi_i Q_{ij} \frac{\frac{p_j}{\pi_j} - \frac{p_i}{\pi_i}}{\log \frac{\pi_i p_j}{\pi_j p_i}} (\psi_i - \psi_j), \\ \frac{d\psi_i}{dt} + \gamma(t)\psi_i + \frac{1}{2} \sum_{j \neq i} Q_{ij} \left[\log \left(\frac{\pi_j p_i}{\pi_i p_j} \right) + 1 - \left(\frac{\pi_j p_i}{\pi_i p_j} \right)^{-1} \right] \\ + \frac{1}{2} \sum_{j \neq i} Q_{ij} \frac{\log \left(\frac{\pi_j p_i}{\pi_i p_j} \right) - 1 + \left(\frac{\pi_j p_i}{\pi_i p_j} \right)^{-1}}{\log^2 \left(\frac{\pi_j p_i}{\pi_i p_j} \right)} (\psi_i - \psi_j)^2 = 0. \end{cases} \quad (31)$$

We will refer to this approach as the **log-Fisher** method. One advantage of this method is that it preserves the positivity of $p(t)$ along the damped Hamiltonian flow, whereas the KL method does not.

3.4 The Relative Fisher Information and Constant Activation

Now we consider a constant mobility weight matrix (θ_{ij}) that does not depend on $p(t)$, whose entries are positive. Selecting $\mathcal{U}(p) = \frac{1}{4} \sum_{i,j=1}^n \omega_{ij} \theta_{ij} (\log \frac{p_i}{\pi_i} - \log \frac{p_j}{\pi_j})^2$, (21) reads

$$\begin{cases} \frac{dp_i}{dt} = \sum_{j \neq i} \pi_i Q_{ij} \theta_{ij} (\psi_i - \psi_j), \\ \frac{d\psi_i}{dt} + \gamma(t)\psi_i + \frac{\pi_i}{p_i} \sum_{j \neq i} Q_{ij} \theta_{ij} \log \left(\frac{\pi_j p_i}{\pi_i p_j} \right) = 0. \end{cases}$$

We refer this as the **con-Fisher** method. This potential $\mathcal{U}(p)$ inherits the advantages discussed in the Section 3.3 such as the unique critical point and preserving strict positivity, while simplifying ψ -equation (21b). Additionally, the Hessian of $\mathcal{U}(p)$ takes a simpler form compared to the one in **log-Fisher**. A detailed analysis will be presented in Section 4.4.

4 Properties of aMCMC

In this section we discuss key properties of aMCMC and compare advantages and disadvantages across different methods.

4.1 Normalizing Constant

To design a damped Hamiltonian system (19) that does not require the normalizing constant Z , it is necessary to verify the following conditions:

- The Onsager's response matrix $\mathbb{K}(p)$ defined in (9) is independent of Z .
- π is the unique critical point to $\mathcal{U}(p)$ in $\mathbb{P}(V)$.

- The damping parameter $\gamma(t)$ does not rely on the knowledge of Z .

In **Chi-Squared** and **con-Fisher** methods, the associated Onsager response matrix $K_{ij} = -\omega_{ij}\theta_{ij}$ is constant, where parameters are commonly selected as $\omega_{ij} = \pi_i Q_{ij}^{\text{MH}}$ and $\theta_{ij} = 1$. Though Q^{MH} itself is independent of Z , the resulting K depends on Z . In contrast, **KL** and **log-Fisher** methods take the Onsager response matrix in the form of $K_{ij}(p) = -\pi_i Q_{ij}^{\text{MH}} \frac{\frac{p_i}{\pi_i} - \frac{p_j}{\pi_j}}{\log \frac{\frac{p_j}{\pi_j} p_i}{\pi_i p_j}} = -Q_{ij}^{\text{MH}} \frac{p_i - p_j \frac{\pi_i}{\pi_j}}{\log \frac{\frac{p_j}{\pi_j} p_i}{\pi_i p_j}}$, which does not depend on Z .

4.2 Positivity

The χ^2 divergence $\frac{1}{2} \sum_{i=1}^n \frac{(p_i - \pi_i)^2}{\pi_i}$ and the KL divergence $\sum_{i=1}^n p_i \log \frac{p_i}{\pi_i}$ remain well-defined even if some state $p_i = 0$. However, neither divergence explicitly prevents $p_i(t)$ from approaching zero during evolution. In the following theorem, we propose a general condition on the function $\mathcal{U}(p)$ to ensure $p_i(t)$ away from zero. The potentials in **log-Fisher** and **con-Fisher** are two examples.

Theorem 4 *Given a strictly positive target probability π and an irreducible transition-rate matrix Q , let $(p(t), \psi(t))$ be the solution to the damped Hamiltonian dynamics (21) on a graph $G = (V, E, \omega)$, with the potential function $\mathcal{U}(p)$ in the form of*

$$\mathcal{U}(p) = \frac{1}{4} \sum_{i,j=1}^n F_{\frac{p_i}{\pi_i}} \left(\frac{p_j}{\pi_j} \right) \omega_{ij},$$

where $F_{r_0}(r) : \mathbb{R}_+ \mapsto \mathbb{R}$ is a family of functions with a parameter $r_0 \in \mathbb{R}_+$, satisfying that

- 1) $F_{r_0}(r) \geq 0$ with the equality if and only if $r = r_0$.
- 2) $\lim_{r \rightarrow 0^+} F_{r_0}(r) = \infty$.
- 3) $F_{r_0}(r)$ is strictly decreasing on $(0, r_0]$.
- 4) Fix $r \in (0, r_0]$, if $r_1 > r_0$, then $F_{r_1}(r) > F_{r_0}(r)$.

Suppose $\mathcal{H}(p(0), \psi(0))$ is bounded and $p(0) > 0$, then there exists a positive constant $\varepsilon > 0$, such that for any t and for any i , $p_i(t) > \varepsilon$.

Example 1 In Section 3.3, $\mathcal{U}(p) = \frac{1}{4} \sum_{i,j=1}^n (\log \frac{p_i}{\pi_i} - \log \frac{p_j}{\pi_j}) (\frac{p_i}{\pi_i} - \frac{p_j}{\pi_j}) \omega_{ij}$ corresponds to $F_{r_i}(r_j) = (\log r_i - \log r_j)(r_i - r_j)$ and $r_i = \frac{p_i}{\pi_i}$.

Example 2 In Section 3.4, $\mathcal{U}(p) = \frac{1}{4} \sum_{i,j=1}^n (\log \frac{p_i}{\pi_i} - \log \frac{p_j}{\pi_j})^2 \theta_{ij} \omega_{ij}$ chooses $F_{r_i}(r_j) = (\log r_i - \log r_j)^2 \theta_{ij}$ for some positive constant matrix (θ_{ij}) and $r_i = \frac{p_i}{\pi_i}$.

One can verify conditions in Theorem 4 are satisfied in both examples. The proof can be found in Appendix E.

4.3 Damping Parameter and Convergence Analysis

With the Onsager's response matrix $\mathbb{K}(p)$ in (9), our proposed dynamics (21) become

$$\begin{cases} \dot{p}(t) = \psi(t)\mathbb{K}(p(t)), \\ \dot{\psi}(t) = -\frac{1}{2}\nabla_p\langle\psi(t), \psi(t)\mathbb{K}(p(t))\rangle - \gamma(t)\psi(t) - \nabla_p\mathcal{U}(p(t)). \end{cases}$$

Recall the Hamiltonian is $\mathcal{H}(p, \psi) = \frac{1}{2}\psi\mathbb{K}(p)\psi^\top + \mathcal{U}(p)$.

In this subsection, we establish the exponential convergence of the state variables for an explicitly chosen damping parameter by employing the Lyapunov analysis. Previous work designs the damping parameter $\gamma(t)$ using the minimum Hessian eigenvalue in Euclidean settings (Nesterov, 1983, 2004) or sectional curvatures on Riemannian manifolds (Alimisis et al., 2020). When the Onsager response matrix $\mathbb{K}(p)$ depends on p , analyzing sectional curvatures on the probability manifold $\mathbb{P}(V)$ endowed with the graphical Wasserstein metric g_W becomes essential (Li, 2025).

Our derivation relies on the assumptions that the Onsager's response matrix is constant (i.e, independent of $p(t)$), and the potential function $\mathcal{U}(p)$ is geodesically λ -strongly convex. Let the Onsager's response matrix $\mathbb{K}(p) = K$ for some positive semi-definite K . The corresponding Riemannian metric is flat. A function \mathcal{U} on $\mathbb{P}(V)$ equipped with such a flat metric is geodesically λ -strongly convex for some constant $\lambda > 0$, if

$$\mathcal{U}(\hat{p}) \geq \mathcal{U}(p) + (\hat{p} - p)\nabla_p\mathcal{U}(p)^\top + \frac{\lambda}{2}\|\hat{p} - p\|_{K^\dagger}^2. \quad (32)$$

Now, we define a Lyapunov function by

$$\mathcal{L}(t) = \frac{1}{2}e^{\sqrt{\lambda}t}\|\sqrt{\lambda}(p(t) - \pi) + \psi K\|_{K^\dagger}^2 + e^{\sqrt{\lambda}t}(\mathcal{U}(p(t)) - \mathcal{U}(\pi)). \quad (33)$$

Theorem 5 *Consider the probability manifold $\mathbb{P}(V)$ on a graph $G = (V, E, \omega)$ equipped with a flat metric (11) or (13), induced from a constant Onsager's response matrix (9). Given a function \mathcal{U} that is geodesically λ -strongly convex for $\lambda > 0$, select a time-homogeneous damping parameter $\gamma(t) = 2\sqrt{\lambda}$, and let $(p(t), \psi(t))$ be the solution to the proposed damped Hamiltonian dynamics (19). Then the Lyapunov function (33) is non-increasing. Furthermore, $\mathcal{U}(p(t)) - \mathcal{U}(\pi) \leq \mathcal{O}(e^{-\sqrt{\lambda}t})$.*

Proof

$$\begin{aligned} e^{-\sqrt{\lambda}t}\frac{d\mathcal{L}}{dt} &= \frac{1}{2}\sqrt{\lambda}\left[\lambda\|p - \pi\|_{K^\dagger}^2 + \|\psi\|_K^2 + 2\sqrt{\lambda}\psi(p - \pi)^\top\right] + \sqrt{\lambda}(\mathcal{U}(p) - \mathcal{U}(\pi)) \\ &\quad + \nabla_p\psi K\mathcal{U}(p)^\top - (\sqrt{\lambda}\psi K + \nabla_p\mathcal{U}(p)K)K^\dagger(\sqrt{\lambda}(p - \pi) + \psi K) \\ &= \frac{1}{2}\lambda^{\frac{3}{2}}\|p - \pi\|_{K^\dagger}^2 + \frac{\sqrt{\lambda}}{2}\|\psi\|_K^2 + \lambda\psi(p - \pi)^\top + \sqrt{\lambda}(\mathcal{U}(p) - \mathcal{U}(\pi)) + \psi K\nabla_p\mathcal{U}(p)^\top \\ &\quad - \lambda\psi(p - \pi)^\top - \sqrt{\lambda}\|\psi\|_K^2 - \sqrt{\lambda}(p - \pi)\nabla_p\mathcal{U}(p)^\top - \psi K\nabla_p\mathcal{U}(p)^\top \\ &= -\frac{1}{2}\sqrt{\lambda}\|\psi\|_K^2 + \sqrt{\lambda}\left[\mathcal{U}(p) - \mathcal{U}(\pi) + (\pi - p)\nabla_p\mathcal{U}(p)^\top + \frac{\lambda}{2}\|\pi - p\|_{K^\dagger}^2\right]. \end{aligned} \quad (34)$$

Observe that the first term in (34) is non-positive. The second term in (34) is also non-positive by the geodesically λ -strongly convex assumption on \mathcal{U} . Thus, we conclude that $\frac{d\mathcal{L}}{dt} \leq 0$, which implies

$$\mathcal{U}(p(t)) - \mathcal{U}(\pi) \leq e^{-\sqrt{\lambda}t} \mathcal{L}(t) \leq e^{-\sqrt{\lambda}t} \mathcal{L}(0) = \mathcal{O}(e^{-\sqrt{\lambda}t}).$$

■

4.4 Geodesic Convexity, Hessian and Eigenvalues

According to Theorem 5, under the flat metric K , the damping parameter $\gamma(t)$ can be designed based on the constant $\lambda > 0$ that characterizes the convexity of \mathcal{U} . Appendix D reviews the relation between the Hessian and geodesic convexity of a potential \mathcal{U} , following Mielke (2013). It suffices to verify condition (32) or to establish that $D^2\mathcal{U} \succeq \lambda K^\dagger$ for some constant $\lambda > 0$. In this section, we study how to find the constant λ .

4.4.1 CHI-SQUARED METHOD

To check if $\mathcal{U}(p) = \frac{1}{2} \sum_{i=1}^n \frac{(p_i - \pi_i)^2}{\pi_i}$ is geodesically λ -strongly convex, we need to find a positive constant $\lambda > 0$ such that

$$\begin{aligned} \mathcal{U}(\hat{p}) - \mathcal{U}(p) - (\hat{p} - p)(\nabla_p \mathcal{U}(p))^\top &= \sum_{i=1}^n (\hat{p}_i - p_i) \frac{\hat{p}_i + p_i - 2\pi_i}{2\pi_i} - \sum_{i=1}^n (\hat{p}_i - p_i) \frac{p_i - \pi_i}{\pi_i} \\ &= \sum_{i=1}^n (\hat{p}_i - p_i) \frac{\hat{p}_i - p_i}{2\pi_i} = (\hat{p} - p) \text{diag}\left(\frac{1}{2\pi}\right) (\hat{p} - p)^\top \geq \frac{\lambda}{2} (\hat{p} - p) K^\dagger (\hat{p} - p)^\top, \end{aligned}$$

where $K = -\omega = -\text{diag}(\pi)Q$. A sufficient condition is that $0 < \lambda \leq \frac{\min \frac{1}{\pi_i}}{\lambda_{\max}((- \omega)^\dagger)}$. Given that π is assumed to be strictly positive and ω is the weight matrix associated to a reversible and irreducible Markov chain, we know λ exists.

Given a transition rate matrix Q , for instance Q^{MH} in MH, we compare the convergence of the classical MCMC method and its accelerated counterpart driven by the χ^2 divergence, using spectral analysis. In particular, when a constant damping parameter is applied, the matrix L defined in (27) is a constant matrix, whose eigenvalues can be computed directly. In Lemma 6 we derive an explicit relationship between the spectrum of L and Q , which enables a quantitative comparison of convergence rates in terms of the spectral gap in Theorem 7. Background material on the spectral properties of general irreducible and reversible transition rate matrices is provided in Appendix B.

Lemma 6 *Let $\gamma(t) = d$ for some $d > 0$.*

- *If μ is a real eigenvalue of L , then $\alpha = \mu(d + \mu)$ is a real eigenvalue of Q .*
- *If α is a real eigenvalue of Q , then there exist (possibly complex) eigenvalues μ of L such that $\mu(d + \mu) = \alpha$.*

Proof Given square matrices A, B, C, D , if C, D are commutative, then we have the simple determinant formula

$$\det \begin{pmatrix} A & B \\ C & D \end{pmatrix} = \det(AD - BC).$$

Take $A = 0_{n \times n}$, $B = -\text{diag}(\frac{1}{\pi})$, $C = -\text{diag}(\pi)Q$, and $D = -dI_n$ from L matrix in (27), then

$$\det(L - \mu I_{2n}) = \det((A - \mu I_n)(D - \mu I_n) - BC) = \det(\mu(d + \mu)I_n - Q). \quad (35)$$

Obviously, if μ is a real eigenvalue of L , then $\alpha = \mu(d + \mu)$ is a real eigenvalue of Q . On the other hand, if α is a real eigenvalue of Q , there exists (possibly complex) μ such that $\mu(d + \mu) = \alpha$, and

$$0 = \det(\alpha I_n - Q) = \det(\mu(d + \mu)I_n - Q) = \det(L - \mu I_{2n}).$$

■

In particular, 0 is an eigenvalue of both Q and L .

Theorem 7 Let α_* be the largest negative eigenvalue (i.e., the spectral gap) of Q ,

$$\alpha_* = \max \{ \alpha < 0 \mid (Q - \alpha I) \text{ is not injective} \}.$$

If $|\alpha_*| < 1$, then there exists damping parameter $\gamma(t) = d \in [2\sqrt{|\alpha_*|}, |\alpha_*| + 1)$, such that the largest negative eigenvalue μ_* of L satisfies $\mu_* < \alpha_*$.

Proof Let α be an eigenvalue of Q , then from (35) there exists $\mu_1(\alpha) = \frac{-d + \sqrt{d^2 + 4\alpha}}{2}$, $\mu_2(\alpha) = \frac{-d - \sqrt{d^2 + 4\alpha}}{2}$ which are (possibly complex) eigenvalues of L . In particular, $\mu_1(0) = 0$ and $\mu_2(0) = -d$. Let $\alpha_{n-1} \leq \alpha_{n-2} \leq \dots \leq \alpha_1 < 0 = \alpha_0$ denote the ordered eigenvalues of Q . Then $\alpha_* = \alpha_1$. Fix $\alpha \in [\alpha_{n-1}, \alpha_1]$. If $d \geq 2\sqrt{|\alpha|}$, then $\mu_2(\alpha) \leq -\frac{d}{2} \leq \mu_1(\alpha) < 0$. If $d < 2\sqrt{|\alpha|}$, $\text{Re}(\mu_1(\alpha)) = \text{Re}(\mu_2(\alpha)) = \frac{-d}{2}$. Since $|\alpha_*| < 1$, we can pick $d \in [2\sqrt{|\alpha_*|}, |\alpha_*| + 1)$. We consider two cases:

- If there exists some k such that $d \in [2\sqrt{|\alpha_k|}, 2\sqrt{|\alpha_{k+1}|})$, then

$$\mu_1(\alpha_1) = \max \{ \mu_1(\alpha_1), \mu_2(\alpha_1), \dots, \mu_1(\alpha_k), \mu_2(\alpha_k) \} \geq -\frac{d}{2},$$

while $\text{Re}(\mu_1(\alpha_j)) = \text{Re}(\mu_2(\alpha_j)) = -\frac{d}{2}$ for $j \geq k + 1$. Thus $\mu_* = \mu_1(\alpha_*) = \frac{-d + \sqrt{d^2 + 4\alpha_*}}{2}$.

- If $2\sqrt{|\alpha_{n-1}|} \leq d < |\alpha_*| + 1$, then $\mu_* = \mu_1(\alpha_*) = \frac{-d + \sqrt{d^2 + 4\alpha_*}}{2}$.

In either case, note that $\mu_* = \frac{-d + \sqrt{d^2 + 4\alpha_*}}{2}$ is increasing w.r.t d . Thus $d < |\alpha_*| + 1$ implies that $\mu_* < \alpha_*$. ■

Remark 8 The optimal choice is in the form of $d = 2\sqrt{|\alpha_*|}$, which resembles the choice of the damping parameter in the classical Nesterov's acceleration (17), and also our choice of $\gamma(t)$ in Theorem 5. It is worth noting that α_* refers to the largest negative eigenvalue of Q in (3), while λ in the Nesterov's method as well as Theorem 5 refers to the λ -strong convexity of the function, satisfying $0 < \lambda \leq \frac{\min_i \frac{1}{\pi_i}}{\lambda_{\max}((- \omega)^{\dagger})}$.

With the optimal damping parameter, $\mu_* = -\sqrt{|\alpha_*|}$ is the optimal convergence rate of Chi-squared method in terms of spectral analysis.

4.4.2 CON-FISHER METHOD

To check if $\mathcal{U}(p) = \mathbb{I}(p|\pi) = \frac{1}{4} \sum_{i=1}^n \sum_{j \neq i} \omega_{ij} \theta_{ij} (\log \frac{p_i}{\pi_i} - \log \frac{p_j}{\pi_j})^2$ is geodesically λ -strongly convex, we need to find a positive constant λ such that

$$\begin{aligned}
 & \mathbb{I}(\hat{p}|\pi) - \mathbb{I}(p|\pi) - (\hat{p} - p) \nabla_p \mathbb{I}(p|\pi) \\
 &= \frac{1}{4} \sum_{i=1}^n \sum_{j \neq i} \omega_{ij} \theta_{ij} \left[\log \frac{\pi_j^2 p_i \hat{p}_i}{\pi_i^2 p_j \hat{p}_j} \log \frac{\hat{p}_i p_j}{p_i \hat{p}_j} \right] - \sum_{i=1}^n (\hat{p}_i - p_i) \frac{\pi_i}{p_i} \sum_{j \neq i} Q_{ij} \theta_{ij} \log \frac{\pi_j p_i}{\pi_i p_j} \\
 &= \sum_{i=1}^n \sum_{j \neq i} \omega_{ij} \theta_{ij} \left[\frac{1}{4} \log \left(\frac{\hat{p}_i p_j}{p_i \hat{p}_j} \right)^2 + \frac{1}{2} \log \left(\frac{\hat{p}_i p_j}{p_i \hat{p}_j} \right) \log \frac{\pi_j p_i}{\pi_i p_j} - \left(\frac{\hat{p}_i}{p_i} - 1 \right) \log \frac{\pi_j p_i}{\pi_i p_j} \right] \\
 &\geq \frac{\lambda}{2} (\hat{p} - p) K^\dagger (\hat{p} - p)^\top,
 \end{aligned}$$

where $K = (K_{ij})$ and $K_{ij} = -\omega_{ij} \theta_{ij}$. It seems nontrivial to find a sufficient condition at this moment. Thus we compute the Hessian $D^2\mathcal{U}$ instead. Appendix D provides detailed derivations of the explicit form of the Hessian and its related properties.

The positive constant λ can be obtained by studying the Rayleigh quotient problem

$$\min_{\psi \mathbf{1}_n^\top = 0} \frac{\psi K D^2 \mathcal{U}(p) K^\top \psi^\top}{\psi K \psi^\top}, \quad (36)$$

which can be reformulated as an eigenvalue problem from a computational standpoint; see Appendix D for details.

Lemma 9 *Given a strictly positive target probability π and an irreducible transition-rate matrix Q , we consider the probability manifold $\mathbb{P}(V)$ on a graph $G = (V, E, \omega)$, with the potential $\mathcal{U}(p) = \mathbb{I}(p|\pi) = \frac{1}{4} \sum_{i=1}^n \sum_{j \neq i} \omega_{ij} \theta_{ij} (\log \frac{p_i}{\pi_i} - \log \frac{p_j}{\pi_j})^2$, where (θ_{ij}) is a constant matrix whose entries are positive.*

Let $K = (K_{ij})$ be the associated Onsager's response matrix, where $K_{ij} = -\omega_{ij} \theta_{ij}$ and $K_{ii} = -\sum_{j \neq i} K_{ij}$. Then there exists a positive constant λ such that $D^2\mathcal{U}(p)|_{p=\pi} \geq \lambda K^\dagger$.

Consequently, we may use this λ computed from **con-Fisher** at stationary distribution $p = \pi$ to construct the asymptotical limit of the damping parameter $\gamma(t) = 2\sqrt{\lambda}$ in the **log-Fisher** method.

5 Numerical Schemes

In this section, we outline numerical schemes employed in subsequent numerical experiments for the ODE integrator of (21) and the jump process associated with (23), (24) in aMCMC.

5.1 ODE Integrator

The classical Hamiltonian Monte Carlo (HMC), requires specialized discretization schemes, such as the symplectic Euler scheme for volume-preserving or the Leapfrog scheme for quantity-conserving (see Neal, 2011). For our proposed damped Hamiltonian dynamics

(21), we adopt the staggered scheme with splitting methods. Specifically, given a prescribed damping parameter $\gamma(t)$, we can express (21) as:

$$\begin{cases} \frac{dp(t)}{dt} = A(p(t), \psi(t)), \\ \frac{d\psi(t)}{dt} = B(p(t), \psi(t), \gamma(t)), \end{cases}$$

where $A(p(t), \psi(t)) = \partial_\psi \mathcal{H}(p(t), \psi(t))$ and $B(p(t), \psi(t), \gamma(t)) = -\gamma(t)\psi(t) - \partial_p \mathcal{H}(p(t), \psi(t))$. The associated staggered scheme is given by

$$\begin{cases} \frac{p^{(k+1)} - p^{(k)}}{\Delta t} = A(p^{(k)}, \psi^{(k)}), & (37a) \\ \frac{\psi^{(k+1)} - \psi^{(k)}}{\Delta t} = B(p^{(k+1)}, \psi^{(k)}, \gamma^{(k)}). & (37b) \end{cases}$$

When \mathbb{K} does not depend on p , the Hamiltonian $\mathcal{H}(p, \psi)$ is separable. Thus (37) is indeed the symplectic Euler scheme. Note that (37) involves designing an interacting particle system, which requires simultaneously integrating the coupled system of all state variables and momentum variables. In contrast, the ODE solver of the forward master equation (3) in the MH can integrate each state variable independently.

Since the Hamiltonian $\mathcal{H}(p, \psi)$ is known to decay along the dynamics according to (22), it is therefore natural to employ a numerical scheme that preserves this dissipation property. In our numerical experiments, we select a sufficiently small step size to numerically approximate this continuous-time decay property.

5.2 Jump Process

For the forward master equation (21a), an equivalent form (23) is proposed for the jump process of state variables. Consequently, both classical MH update and the proposed aMCMC admit the transition matrix of the form $P = I_n + Q\Delta t$, where MH takes $Q = Q^{\text{MH}}$ in (5) and aMCMC takes $Q = \bar{Q}_\psi^r$ in (24). The step size Δt is chosen sufficiently small to ensure that all entries of P are nonnegative.

The construction of \bar{Q}_ψ^r requires components $p_i(t)$ to remain strictly positive. This property is guaranteed by Theorem 4 for **log-Fisher** and **con-Fisher** methods. In practical computations, we additionally employ *restart* techniques, detailed in Section 6, to correct potential degeneracies $p_i(t) = 0$ due to random sampling.

Since most target distributions in our numerical experiments are multimodal, as stated in Remark 1, we implement the Metropolis-Hastings jump process in a multi-chain setting, to mitigate sensitivity to poor initialization of a single long chain. This implementation is described in Algorithm 2 and serves as a baseline for comparison with aMCMC, based on approximations to their forward master equations.

In contrast to MH, the aMCMC transition-rate matrix \bar{Q}_ψ^r is time-inhomogeneous and depends on both the empirical distribution $p(t)$ and momentum variables $\psi(t)$, indicating that particles are interacting and exchanging information from the histograms. While the state variables evolve via a jump process, there is no corresponding jump-process formulation for the momentum variable, thus we employ the ODE integrator to solve (37b).

Algorithm 2: Metropolis–Hastings Sampling in Multiple Chains

Input : Initial distribution $p^{(0)}$; transition rate matrix Q^{MH} ; total number of states n ; number of particles M ; step size Δt ; total iterations N .

Output: Terminal distribution $p^{(N)}$.

1 **Initialize:** Transition probability matrix

$$P^{\text{MH}} \leftarrow I_n + Q^{\text{MH}} \Delta t.$$

Sample: Draw M particles according to $p^{(0)}$, and record state counts:

$$\text{bin}(i) \leftarrow \#\{\text{particles in state } i\}, \quad i = 1, \dots, n.$$

2 **for** $k \leftarrow 1$ **to** N **do**

3 **for** $s \leftarrow 1$ **to** n **do in parallel**

 // Simulate transitions from state s

4 Draw $\text{bin}(s)$ samples from $\{1, \dots, n\}$ with probabilities $P^{\text{MH}}(s, :)$;

5 Record the number of arrivals into each state i :

$$\text{tmp}(s, i) \leftarrow \#\{\text{particles jumping from } s \text{ to } i\}.$$

6 **end**

 // Aggregate arrivals across all source states

7

$$\text{bin}(i) \leftarrow \sum_{s=1}^n \text{tmp}(s, i), \quad i = 1, \dots, n.$$

8 **end**

9 **Return:** Terminal distribution

$$p^{(N)} \leftarrow \frac{1}{M} \text{bin}.$$

Algorithm 3: Accelerated MCMC (aMCMC) Sampling

Input : Initial distribution $p^{(0)}$; transition rate matrix Q ; total number of states n ; number of particles M ; step size Δt ; warm-start iterations L ; total iterations N .

Output: Terminal distribution $p^{(N)}$.

- 1 **Warm-start:** Run L iterations of Algorithm 2 starting from $p^{(0)}$, and obtain $p^{(L)}$. Initialize $\psi^{(L)}$ using the strategy depending on the mobility weight matrix (θ_{ij}) .
- 2 **Initialize:** Time-inhomogeneous transition probability matrix $P \leftarrow I_n + \bar{Q}_\psi^r \Delta t$, where the new transition rate matrix \bar{Q}_ψ^r in (24) is constructed from $p^{(L)}$ and $\psi^{(L)}$.
- 3 **Sample:** Draw M particles according to $\rho^{(L)}$, and record state counts

$$\text{bin}(i) \leftarrow \#\{\text{particles in state } i\}, \quad i = 1, \dots, n.$$

- 4 **for** $k \leftarrow L + 1$ **to** N **do**
- 5 **for** $s \leftarrow 1$ **to** n **do in parallel**
 - 6 // Simulate transitions from state s
 - 6 Draw $\text{bin}(s)$ samples from $\{1, \dots, n\}$ with probabilities $P(s, :)$;
 - 7 Record the number of arrivals into each state i :

$$\text{tmp}(s, i) \leftarrow \#\{\text{particles jumping from } s \text{ to } i\}.$$
- 8 **end**
- 9 // Aggregate arrivals across all source states

$$\text{bin}(i) \leftarrow \sum_{s=1}^n \text{tmp}(s, i), \quad i = 1, \dots, n.$$
- 9 // Restart mechanism
- 10 **if** restart condition is triggered due to any empty $\text{bin}(k)$ **then**
- 11 Add particles to all empty bin ;
- 12 Update $p_i^{(k)} \leftarrow \frac{1}{M_k} \text{bin}(i)$, where M_k denotes the current total number of particles at the k -th step;
- 13 Reinitialize all momentum variables $\psi^{(i)}$ according to the restart strategy.
- 14 **else**
- 15 Update $p_i^{(k)} \leftarrow \frac{1}{M_k} \text{bin}(i)$;
- 16 Update $\psi^{(k)}$ via its ODE solver.
- 17 **end**
- 18 Compute \bar{Q}_ψ^r accordingly.
- 18 // Adaptive step-size control (local backtracking)
- 19 $\Delta t^{(k)} \leftarrow \Delta t$;
- 20 **while** $P = I_n + \bar{Q}_\psi^r \Delta t^{(k)}$ is not a valid transition matrix **do**
- 21 $\Delta t^{(k)} \leftarrow \Delta t^{(k)} / 10$;
- 22 $P \leftarrow I_n + \bar{Q}_\psi^r \Delta t^{(k)}$;
- 23 **end**
- 24 **end**
- 25 **Return:** Terminal distribution $p^{(N)}$.

5.3 Initialization and Restart

For the classical MCMC with the MH update, we initialize the state distribution $p(0)$ by a uniform distribution. While it is well known that MCMC methods generally require a *burn-in* period, where the first few iterations are discarded to mitigate the effects of a poor starting point (Geyer, 2011), we retain all iterations in our experiments reported in Section 6. For aMCMC, in addition to initializing the state variables with a uniform distribution, the momentum variables must also be specified. We observe the following relationship:

- $\theta_{ij} = 1$ in **Chi-squared** and **con-Fisher** methods. Under the choice $\psi_j = -\frac{p_j}{\pi_j}$, (21a) becomes

$$\frac{dp_i}{dt} = \psi_i \sum_{j \neq i} \omega_{ij} - \sum_{j \neq i} \psi_j \omega_{ji} = -\frac{p_i}{\pi_i} \sum_{j \neq i} \pi_i Q_{ij} + \sum_{j \neq i} \frac{p_j}{\pi_j} \pi_j Q_{ji} = \sum_{j \neq i} p_j Q_{ji} - p_i Q_{ij},$$

which is precisely the forward master equation for the classical MCMC.

- $\theta_{ij} = \frac{\frac{p_j - p_i}{\pi_j - \pi_i}}{\log \frac{\pi_i p_j}{\pi_j p_i}}$ in **KL** and **log-Fisher** methods. Under the choice $\psi_j = -\log \frac{p_j}{\pi_j}$, (21a) becomes

$$\frac{dp_i}{dt} = \sum_{j \neq i} \left(-\log \frac{p_i}{\pi_i} + \log \frac{p_j}{\pi_j} \right) \frac{\frac{p_i}{\pi_i} - \frac{p_j}{\pi_j}}{\log \frac{p_i}{\pi_i} - \log \frac{p_j}{\pi_j}} \pi_i Q_{ij} = \sum_{j \neq i} \frac{p_j}{\pi_j} \pi_j Q_{ji} - \frac{p_i}{\pi_i} \pi_i Q_{ij},$$

which recovers the forward master equation for the classical MCMC.

Consequently, the state variables in (21a) evolve identically to classical MCMC, once employing the above assignments of momentum variables. This observation allows us to employ classical MCMC as a warm-start for aMCMC. Specifically, after a prescribed number of MH iterations, we initialize the momentum variables, by $\psi_j(0) = -\frac{p_j(0)}{\pi_j}$ for **Chi-squared** and **con-Fisher** methods, or by $\psi_j(0) = -\log \frac{p_j(0)}{\pi_j}$ for **KL** and **log-Fisher** methods.

Given that the target distribution π is strictly positive and the Markov chain is reversible and irreducible, Theorem 4 ensures strict positivity of the state variables $p(t)$ for both the **log-Fisher** and **con-Fisher** methods. It suggests that when $p_i(t)$ approaches zero, there is a sufficiently large momentum to pull $p_i(t)$ away from zero. Nonetheless, in numerical simulations, accumulation of truncation errors and large step sizes could lead to instances where the state variables become zero or even negative.

For the ease of our discussion, denote by $p_{i,\text{ode}}^{(k)}$ the numerical value of $p_i(t)$ in (21) at the k -th iteration using Euler scheme. Denote by $p_{i,\text{jump}}^{(k)}$ the empirical probability density of state i at the k -th iteration, which is calculated by the ratio between the number of particles in state i at the k -th iteration and the total number of particles M . We first opt for adaptive step sizes (see line 20-23 in Algorithm 3) to prevent any state variables $p_{i,\text{ode/jump}}^{(k)}$ from becoming negative. In practice, this is usually sufficient when solving $p_{i,\text{ode}}^{(k)}$ in (21) with **log-Fisher** and **con-Fisher** methods using Euler scheme. However, due to the random sampling following the transition probability matrix $P = I_n + \bar{Q}_\psi^r \Delta t$, a small

sample size M may cause the empirical particle density $p_{i,\text{jump}}^{(k)}$ to become zero even when $p_{i,\text{ode}}^{(k)} > 0$.

Second, if $p_{i,\text{ode}/\text{jump}}^{(k)} = 0$ after some iterations, we employ a simple *restart* mechanism by the MH update that works for any aMCMC method, described below:

Restart (ODE solver): if $p_{i,\text{ode}}^{(k)} = 0$ for some state i , for all state j we set $\psi_{j,\text{ode}}^{(k)} = -\frac{p_{j,\text{ode}}^{(k)}}{\pi_j}$

in **Chi-squared** and **con-Fisher** methods, or $\psi_{j,\text{ode}}^{(k)} = -\log \frac{p_{j,\text{ode}}^{(k)}}{\pi_j}$ in **KL** and **log-Fisher** methods. This choice ensures the $(k+1)$ -th iteration on the state variables effectively runs *one* iteration of the MH update, thereby pulling $p_{i,\text{ode}}$ away from 0.

Restart (jump process): if $p_{i,\text{jump}}^{(k)} = 0$, i.e., the number of particles at state i is zero after random sampling at the k -th iteration, then we add *one* particle to state i . Note that this also increases the total number of particles by *one*. The updated value of $p_{i,\text{jump}}^{(k)}$ is then set to $(M_{\text{old}} + 1)^{-1}$, where M_{old} is the total amount of particles before adding the new particle. Then we set $\psi_{j,\text{jump}}^{(k)} = -\frac{p_{j,\text{jump}}^{(k)}}{\pi_j}$ in **Chi-squared** and **con-Fisher** methods, or $\psi_{j,\text{jump}}^{(k)} = -\log \frac{p_{j,\text{jump}}^{(k)}}{\pi_j}$ in **KL** and **log-Fisher** methods. In our experiments, the **log-Fisher** method barely requires restart.

Multiple iterations of Metropolis–Hastings restarts or the addition of multiple particles can be performed in experiments to ensure the strict positivity of state variables, albeit at the cost of deviating from the proposed damped Hamiltonian flow.

6 Numerical Examples

In this section, we compare the proposed aMCMC with the Metropolis-Hastings method implemented in multi-chains. Our code is available at <https://github.com/silentmovie/AMCMC>. All experiments in this section are conducted in MATLAB on a MacBook Pro M1 Max. Additional experiments performed on the UCSB computing clusters are reported in the appendix.

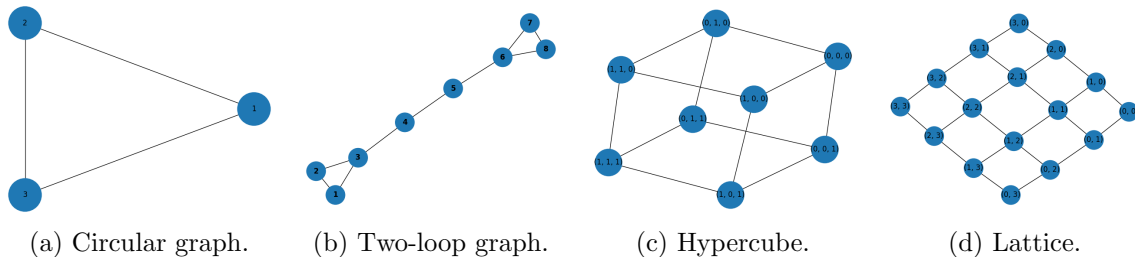


Figure 1: Graph configurations employed in the numerical experiments.

All experiments are conducted on a variety of connected and irreducible graphs, as illustrated in Figure 1. Given a graph $G = (V, E)$, we employ the simple random walk as the candidate kernel, defined by: $q_{ij} = \begin{cases} \frac{1}{\deg(i)} & e_{ij} \in E, \\ 0 & \text{otherwise.} \end{cases}$ The corresponding

Metropolis–Hastings transition rate matrix is constructed as $Q_{ij}^{\text{MH}} = \min \left\{ \frac{\pi_j}{\pi_i} q_{ji}, q_{ij} \right\}$ and the associated weight matrix ω is given by $\omega_{ij} = \pi_i Q_{ij}^{\text{MH}}$. We compare MCMC and aMCMC on the same weighted undirected graph $G = (V, E, \omega)$, using numerical schemes described in Section 5. In what follows, we illustrate two representative methods: the **Chi-squared** method for small-scale graphs, and the **log-Fisher** method for various graph configurations.

Among methods that do not preserve strict positivity, we select **Chi-squared** method over KL method, in order to numerically validate Theorem 7. We then demonstrate the numerical performance of the **log-Fisher** algorithm in comparison with the MH algorithm, highlighting its superior convergence accuracy in the ℓ^2 density norm.

In all experiments, comparisons are conducted with a fixed total number of iterations, and we additionally report comparisons under a fixed wall-clock time in the last experiment, since aMCMC methods may allow adaptive step sizes, so the effective time spans may differ from those of MH algorithms. Convergence speed, the accuracy for approximating the target distribution π as well as its normalizing constant Z are reported.

6.1 Acceleration and Accuracy via Chi-squared Method

We start with a toy example on the circular graph C_3 (see Figure 1a). The target distribution is $\pi = [0.9913, 0.0044, 0.0043]$ for which the largest negative eigenvalue of Q^{MH} is close to zero, more precisely, $\alpha_* \approx -0.5044$. We choose the damping parameter $\gamma(t) = 2\sqrt{|\alpha_*|} = 1.4220$ as suggested by Theorem 7. With this choice, the largest negative eigenvalue of matrix L in (27) is $\mu_* = -0.7102 < \alpha_*$, thereby suggesting an accelerated convergence rate by the **Chi-squared** method.

The parameters for MH and **Chi-squared** methods are chosen identically:

$$\text{sampling size } M = 10^6, \quad \text{step size } \Delta t = 0.1 \text{ or } 0.01, \quad \text{total iterations } N = 650 \text{ or } 6500.$$

We use small step sizes and a large sampling size to accurately approximate the proposed damped Hamiltonian dynamics, as validated by Figure 2a. We initialize $p(0)$ as the uniform distribution and $\psi_j(0) = -\frac{p_j(0)}{\pi_j}$ and the warm-start is not employed in this experiment. Notably, neither adaptive step size adjustment nor restart mechanisms discussed in Section 5.3 were required in these experiments, yielding a consistent effective time span $[0, 65]$ across all examples shown in Figure 2.

Figure 2b and Figure 2c corroborate the theoretical results in Theorem 7 under different step sizes, demonstrating that **Chi-squared** achieves a faster convergence than the MH update in both ODE and jump process. Notably, jump process sampling achieves a higher order of accuracy $\mathcal{O}(\frac{1}{M})$. When a smaller step size is used, as shown in Figure 2c, the numerical dynamics adhere more closely to the damped Hamiltonian, further accelerating convergence.

6.2 Acceleration and Accuracy via log-Fisher Method

Now we test **log-Fisher** method on the other graph configurations in Figure 1. Certain geometric features of a Markov Chain influence its mixing time, with bottlenecks being a notable example (See Levin et al., 2009). A two-loop graph (see Figure 1b) bridged by a thin “bottleneck” is one of those examples. We apply **log-Fisher** method on this configuration

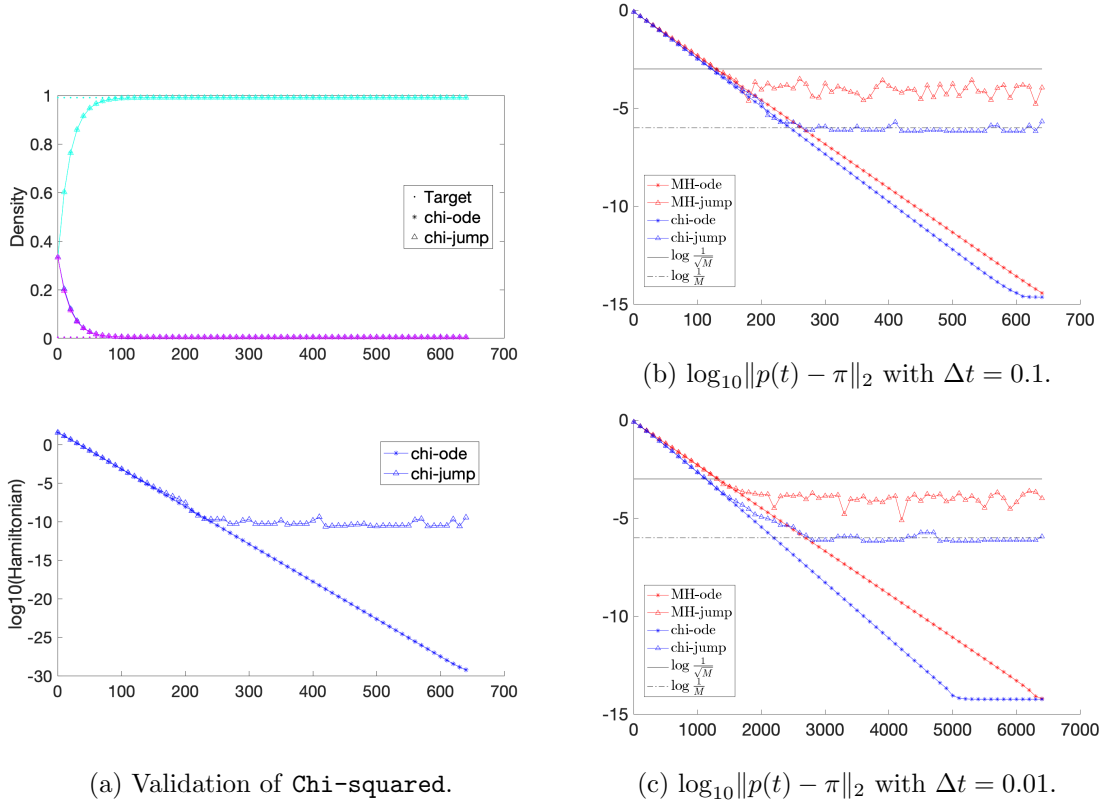


Figure 2: Accelerated sampling on C_3 graph Figure 1a via **Chi-squared** method. x-axes are in iterations and all results are over time span $[0, 65]$ when both ODE solvers achieve machine precision. (a) Validation of the **Chi-squared** method using step size $\Delta t = 0.1$, showing density convergence and the decay of $\log_{10}(\mathcal{H}(p(t), \psi(t)))$. (b) and (c) show the decay of $\log_{10}\|p(t) - \pi\|_2$ for step sizes $\Delta t = 0.1$ and $\Delta t = 0.01$ respectively. Notably, chi-jump achieves an error of order $\mathcal{O}(1/M)$.

first. The target distribution is given by $\pi = [\frac{4}{27}, \frac{4}{27}, \frac{4}{27}, \frac{1}{18}, \frac{1}{18}, \frac{4}{27}, \frac{4}{27}, \frac{4}{27}]$ so that the largest negative eigenvalue to the associated Q^{MH} is small, precisely -3.79×10^{-2} . The parameters for MH and **log-Fisher** methods are chosen identically:

$$\text{sampling size } M = 10^4, \quad \text{step size } \Delta t = 0.1 \quad \text{total iterations } N = 1000.$$

We again initialize $p(0)$ as the uniform distribution and $\psi_j(0) = -\frac{p_j(0)}{\pi_j}$ and the warm-start is not employed in this experiment. In this example, we use the following damping parameter inspired by the Nesterov's accelerated gradient (NAG) method. We also set a lower bound on the damping parameter as suggested by **con-Fisher** method in Section 4.4:

$$\gamma(t) = \begin{cases} 0.5 & t < 3; \\ \max\left\{\frac{3}{t-2}, 0.6\right\} & t \geq 3. \end{cases}$$

With the above choice of parameters, neither restarts nor adaptive step sizes are required in this experiment. Thus we compare the dynamics driven by the relative Fisher information with those by the MH update. As shown in Figure 3, the jump process by the **log-Fisher** method exhibits faster convergence for fixed number of iterations, and achieves higher accuracy than its MH counterpart, particularly once MH sampling reaches its accuracy limit $\mathcal{O}(\frac{1}{\sqrt{M}})$. Although the ODE integrator associated with **log-Fisher** reaches machine precision more slowly than the MH-based integrator, its convergence rate can potentially be accelerated by appropriately tuning the damping parameter.

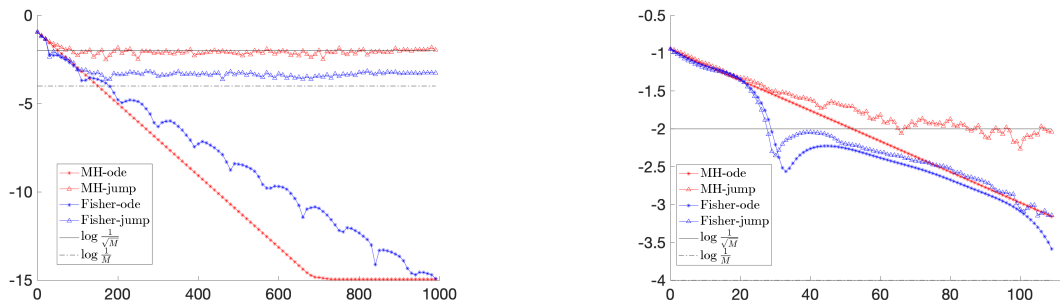


Figure 3: Accelerated sampling on a two-loop graph of node 8 (see Figure 1b) via **log-Fisher** method. x-axes are in iterations with the step size $\Delta t = 0.1$. y-axes is on error $\log_{10} \|p(t) - \pi\|_2$. The right figure zooms in the first 120 iterations of the left figure when the jump process of MH update reaches its accuracy limit $\mathcal{O}(\frac{1}{\sqrt{M}})$. The jump process via **log-Fisher** method exhibits faster convergence and higher accuracy.

In the second example, we compare the jump process on a hypercube graph (see Figure 1c) of 64 nodes. The target distribution is designed to place significant mass at two maximally distant vertices in the hypercube, with the remaining nodes sharing uniformly small mass. Specifically, we set $\pi = \frac{1}{Z}[16, 1, \dots, 1, \dots, 1, 16]$. Note that the normalizing constant Z is not required in **log-Fisher** method. The parameters are specified as follows:

$$\text{sampling size } M = 10^4, \quad \text{step size } \Delta t = 0.01 \quad \text{total iterations } N = 6 \times 10^3.$$

Note that largest negative eigenvalue $\alpha_* \approx -0.0468$ of Q^{MH} . We choose the damping parameter inspired by NAG and **con-Fisher** method as:

$$\gamma(t) = \max \left\{ \frac{2\sqrt{-\alpha_*}}{t}, 0.17 \right\} \quad t \geq 1.$$

In the experiment by the **log-Fisher** method, we run a warm-start of 100 iterations (i.e., $t < 1$) by the MH update to initialize, as described in Section 5.3. Restart or adaptive step sizes are still not activated, thus the comparison between both methods run in the same time span. Though we do not yet know how to select the optimal damping parameter for the **log-Fisher** method, the above conventional choice showcases its acceleration especially when the MH achieves its accuracy limit.

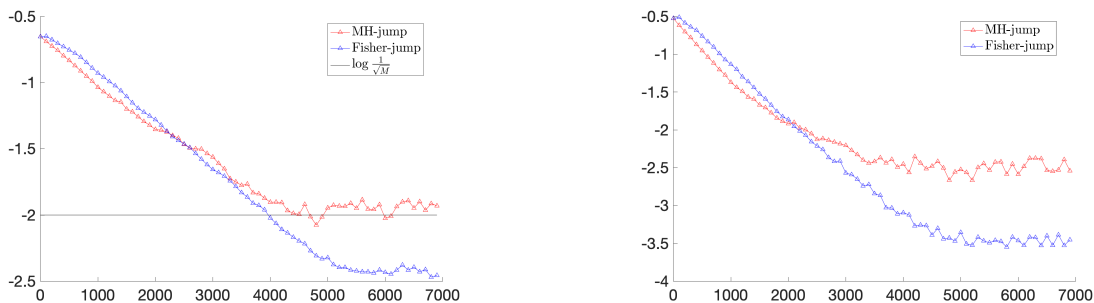


Figure 4: Sampling on a hypercube graph of 64 nodes (see Figure 1c) via **log-Fisher** method. x-axes are in iterations with step size $\Delta t = 0.01$. The left figure shows the approximation error $\log_{10}\|p(t) - \pi\|_2$ w.r.t the target distribution π . The right figure shows the approximation error $\log_{10}|\sum_{i=1}^n p_i(t) \log \frac{p_i(t)}{Z\pi_i} - (-\log Z)|$ w.r.t the normalizing constant Z .

In the next example, we evaluate the performance of jump process on a graph of a large number of nodes. The target distribution is defined as a mixture of two Gaussian distributions on $[0, 1]^2$, discretized a 25×25 lattice graph shown in Figure 1d:

$$\pi(x) = \frac{1}{Z} \left[\exp(-10\|x - x_1\|_2^2) + \exp(-40\|x - x_2\|_2^2) \right], \quad (38)$$

where $x_1 = (0.25, 0.25)$ and $x_2 = (0.75, 0.75)$. This setting poses a challenging multimodal sampling problem. The common parameters are specified as follows:

sampling size $M = 5 \times 10^5$, default step size $\Delta t = 0.01$ total iterations $N = 1.5 \times 10^5$.

For the **log-Fisher** method, we first run a warm-start initialization by the MH update over the first 2999 iterations (i.e., $t < 30$, accounting for 2.00% of the total iterations). After this initialization phase, we employ a constant damping parameter $\gamma(t) = 2\sqrt{\lambda_*} = 0.0065$ for simplicity of the test, where λ_* is obtained from the Rayleigh quotient suggested by the **con-Fisher** method at the asymptotical limit.

Unlike the previous experiments, both adaptive step sizes and restart mechanism are activated for the **log-Fisher** method, to prevent $p_{i,\text{jump}}^{(k)}$ from being zero. The adaptive step-size scheme results in an effective time span of approximately $[0, 1449.9]$, corresponding

to 96.66% of the MH method’s duration. The restart mechanism is activated whenever $p_{i,\text{jump}}^{(k)} = 0$, in which case the damping effect is disabled in the next step. During the entire jump process, the restart mechanism is activated 1243 times (approximately 0.85% of the total iterations). The frequency of restarts per 1000 iterations ranges from 0 to 14.

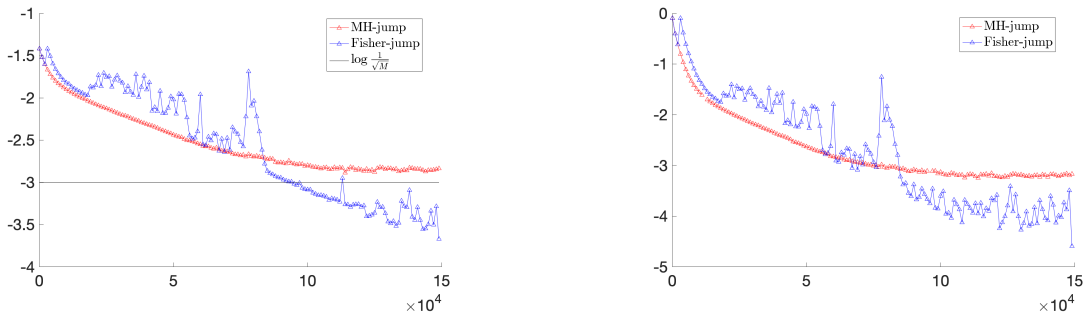


Figure 5: Sampling on a 25×25 lattice graph (see Figure 1d) via **log-Fisher** method for the target distribution as a mixture of two Gaussian distributions. x-axes are in iterations. The left figure shows the approximation error $\log_{10}\|p(t) - \pi\|_2$ w.r.t the target distribution π . The right figure shows the approximation error $\log_{10}|\sum_{i=1}^n p_i(t) \log \frac{p_i(t)}{Z\pi_i} - (-\log Z)|$ w.r.t the normalizing constant Z . The jump process via **log-Fisher** achieves to a higher accuracy when that via MH is approaching to $\mathcal{O}(\frac{1}{\sqrt{M}})$.

As shown in Figure 5, the **log-Fisher** method exhibits faster convergence in terms of iterations, and achieves smaller approximation errors to the target distribution and to the normalizing constant. Figure 6 plots the evolution of the empirical distribution of the state variable.

In the final example, we test the **log-Fisher** method on real datasets used in Xu et al. (2023). In the absence of prior graphical information, we simply read the input images (‘rose’ and ‘fractal tree’) and discretize grayscale images onto a larger lattice of 64×64 nodes. To ensure strict positivity of the target distribution, we add one tenth of the maximum pixel value uniformly to each node. For both target distributions and for experiments conducted using the **log-Fisher** and MH methods, parameters are specified as follows:

$$\text{sampling size } M = 655360, \quad \text{default step size } \Delta t = 0.1 \quad \text{total iterations } N = 2.5 \times 10^4.$$

For the **log-Fisher** method, we first run a warm-start initialization by the MH update over the first 9 iterations (i.e., $t < 1$, or 0.04% of default time span $[0, 2500]$). After that, we employ a constant damping parameter $\gamma(t) = 2\sqrt{\lambda_*}$, where the Rayleigh quotient yields $\lambda_* = 1.7 \times 10^{-6}$ for ‘rose’ example and $\lambda_* = 2.6 \times 10^{-6}$ for ‘fractal tree’. For the ‘rose’ example, the effective time span is $[0, 1279.1]$ due to the adaptive step size and the restart is activated 1478 times (5.91% of total iterations). For the ‘fractal tree’, the effective time span is $[0, 1302.8]$ with 1437 times restart (5.75% of total iterations).

In Figure 7, we compare the empirical distributions obtained at the final iteration, together with the approximation errors for both the target distribution and the normalizing constant, under a fixed number of iterations. A notable difference between two methods on the final sampling results, as shown in Figure 7, is that the empirical distribution generated

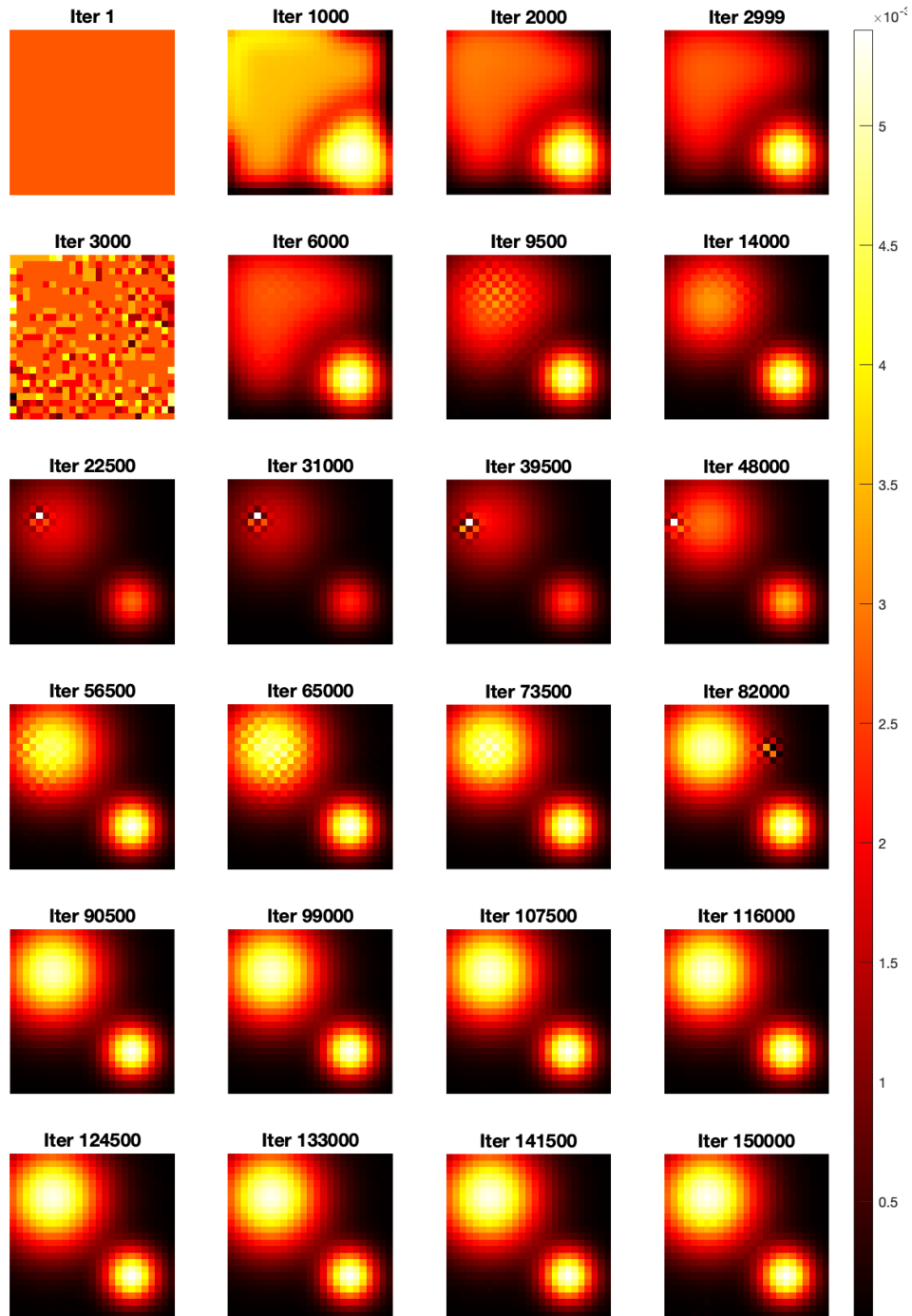


Figure 6: Sampling on a 25×25 lattice for a mixture of two Gaussian distributions supported on $[0, 1]^2$, using the jump process induced by the \log -Fisher method. The abrupt change between the 2999th and 3000th iterations suggests that a more refined choice of the damping parameter and/or the step size may be beneficial. Nonetheless, this simple parameter choice still demonstrates promising performance relative to the MH update.

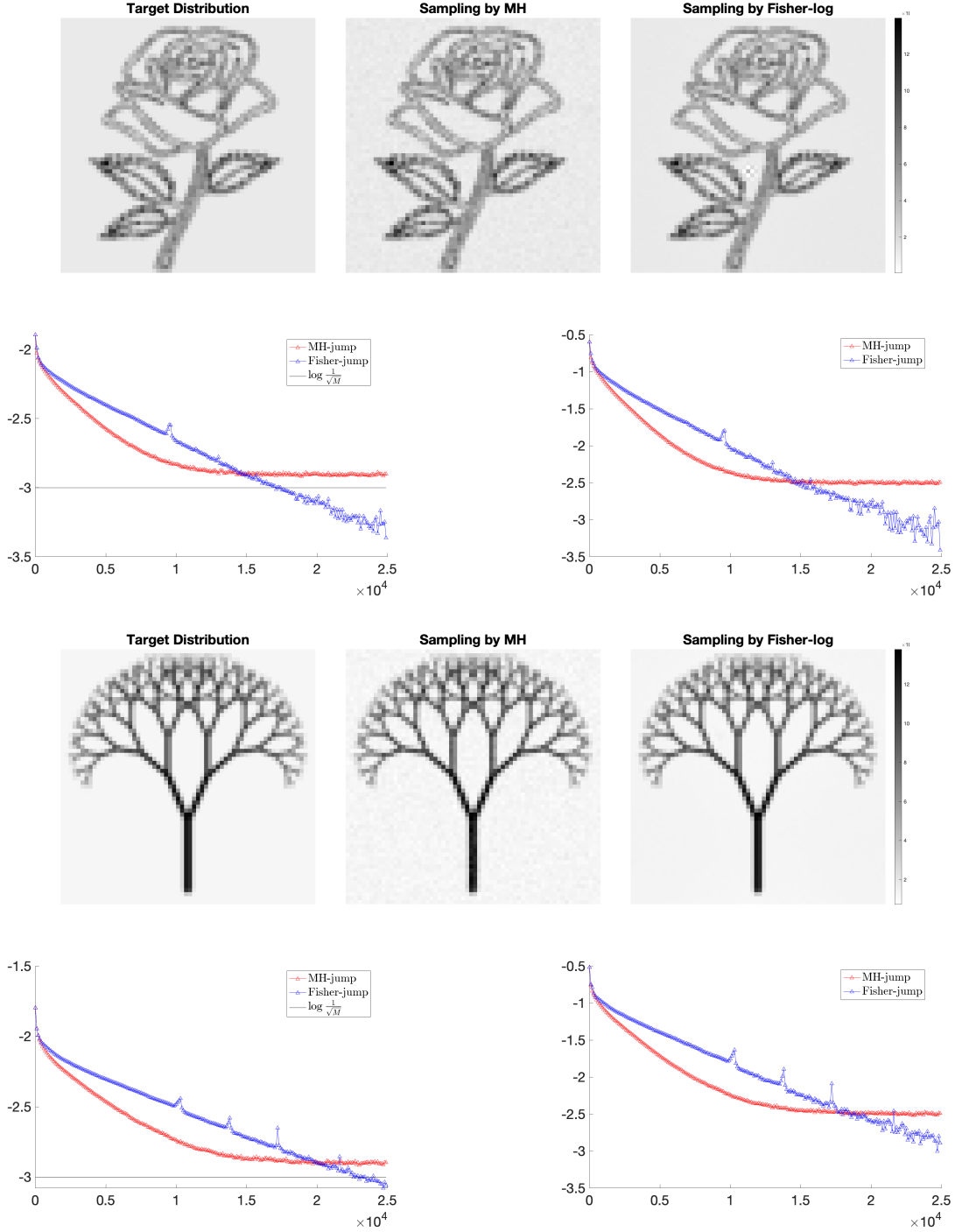


Figure 7: Sampling on a 64×64 lattice graph for real datasets ('rose' and 'fractal tree') via log-Fisher method. Samples are compared at the final iteration. Convergence plots follow the same convention as in previous experiments: x-axes are in iterations; the left plots show the approximation error $\log_{10} \|p(t) - \pi\|_2$ w.r.t the target distribution π ; the right plots show the approximation error $\log_{10} |\sum_{i=1}^n p_i(t) \log \frac{p_i(t)}{Z\pi_i} - (-\log Z)|$ w.r.t the normalizing constant Z .

by our method is smoother. This effect is even more clear in Appendix F, where we provide additional numerical experiments on piecewise constant target distributions. Heuristic observations are also reported.

Notably, the effective time spans of the Fisher-log method for both datasets are approximately half that of MH, suggesting that the proposed damped Hamiltonian dynamics driven by the Fisher information can even outperform the MH method for a fixed wall clock time, as validated in Figure 8. Therefore, A more detailed investigation of refined numerical schemes, including optimized step sizes election, is therefore warranted and left for future work.

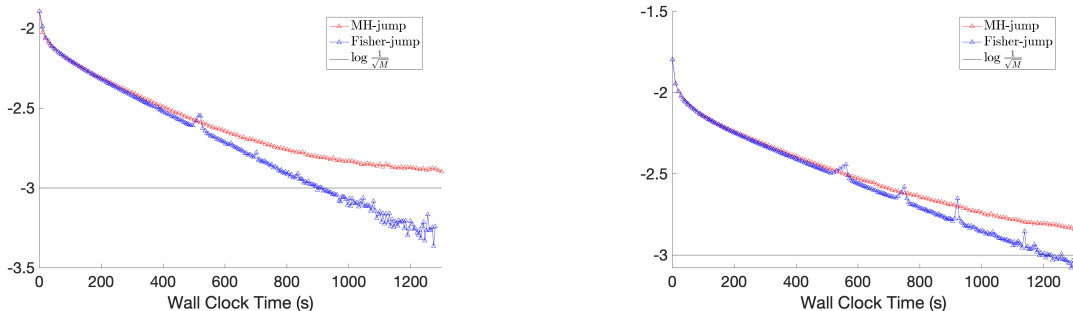


Figure 8: Results from Figure 7 are truncated at 1300 second of wall-clock time. The left is for the ‘rose’ target and the right is for ‘fractal tree’ target. x-axes are wall-clock time (seconds). y-axes are on the approximation error $\log_{10}\|p(t) - \pi\|_2$ w.r.t the target distribution π .

7 Discussions

In this paper, we design accelerated Markov Chain Monte Carlo (aMCMC) algorithms to sample target distributions on a discrete domain, by incorporating Nesterov’s acceleration into the Metropolis-Hastings (MH) algorithm. The MCMC sampling algorithm can be formulated as an optimization problem in the space of probabilities. We study the MH algorithm as a gradient descent method for the KL divergence in the discrete Wasserstein-2 space. Our algorithm utilizes moment-based accelerated gradient methods in discrete Wasserstein-2 spaces and then develops an interacting Markov particle process in discrete domains. Numerical examples on various graphs illustrate the effectiveness of the aMCMC algorithm.

In addition, the proposed accelerated sampling algorithm is related to the score functions on discrete domains. In Lou et al. (2024), the discrete score function $\nabla \log p = \frac{\nabla p}{p}$ is approximated by $[\frac{p_j(t) - p_i(t)}{p_i(t)}]_{j \neq i}$. In this paper, we approximate the score function of a detailed-balanced MCMC algorithm by $\log \frac{p_j}{p_i} = \log p_j - \log p_i$ and the logarithmic mean (2). In future work, we shall study these differences in the approximation of discrete score functions in terms of sampling complexities.

Several open problems arising from the proposed accelerated MCMC framework merit further investigation. First, it is of interest to analyze the choice of the damping parameter

$\gamma(t)$ with a given potential function. The choice of an optimal damping parameter is closely related to the geometric calculations on the generalized Wasserstein-2 manifold (Li, 2025). Second, a study of optimal step-size selection for the current numerical scheme remains open. Alternatively, a finer discretization scheme that allows large time step sizes and its convergence study invite further investigation. Third, it would be natural to incorporate additional acceleration techniques, such as irreversible jump samplers (Ma et al., 2019), into the present framework, with particular emphasis on deriving single-chain approximations of the current swarm-based dynamics. Moreover, another interesting direction is to investigate the efficiency of score estimation in aMCMC. This estimation can be formulated as a variational framework based on time-reversible diffusion on discrete states.

Acknowledgments and Disclosure of Funding

S. Liu, B. Zhou and X. Zuo are supported by AFOSR YIP award No. FA9550-23-1-0087. W. Li is supported by AFOSR YIP award No. FA9550-23-1-0087, NSF RTG: 2038080, NSF FRG: 2245097, and the McCausland Faculty Fellowship at the University of South Carolina. Use was made of the computational facilities administered by the Center for Scientific Computing at the CNSI and MRL (an NSF MRSEC; DMR-2308708) and purchased through NSF CNS-1725797. All authors would like to thank the support of the AMS MRC conference: Ricci Curvatures of Graphs and Applications to Data Science in 2023. The discussion of this manuscript was initiated in the workshop. B. Zhou would like to extend appreciation to Andy Wan for a fruitful discussion. We are also grateful to anonymous reviewers for the incisive comments and suggestions, which improved the quality of this work.

Appendix A. Graph Laplacian and detailed derivation of Wasserstein gradient

Lemma 10 *Suppose the Markov chain is irreducible and reversible with respect to some strictly positive distribution π . Assume $p \in \mathbb{P}(V)$ is strictly positive. Then, the graph Laplacian $\mathbb{K}(p)$ is positive semi-definite with $\text{Ker}(\mathbb{K}(p)) = \text{span}(\mathbb{1}_n)$.*

Proof Recall $\mathbb{K}(p)$ is the graph Laplacian of a weighted undirected graph with a weight matrix $(\omega_{ij}\theta_{ij}(p))$, for any $x = [x_1, \dots, x_n]$, the quadratic form is

$$x\mathbb{K}(p)x^\top = - \sum_{1 \leq i < j \leq n} \mathbb{K}_{ij}(p)(x_i - x_j)^2 = - \sum_{1 \leq i < j \leq n} \omega_{ij}\theta_{ij}(p)(x_i - x_j)^2 \leq 0.$$

The last inequality is due to $\omega_{ij} \geq 0$ and $\theta_{ij}(p) = \frac{\frac{p_i}{\pi_i} - \frac{p_j}{\pi_j}}{f'(\frac{p_i}{\pi_i}) - f'(\frac{p_j}{\pi_j})} > 0$. This verifies that $\mathbb{K}(p)$ is negative definite.

Furthermore, assume $y \in \text{Ker}(\mathbb{K}(p))$, this leads to $y\mathbb{K}(p)y^\top = 0$, which further leads to $\mathbb{K}_{ij}(p)(y_i - y_j)^2 = 0$ for any $1 \leq i < j \leq n$.

Recall that the Markov chain is reducible; for arbitrary $1 \leq k < l \leq n$, we can find a path of nodes $k = i_1 \rightarrow i_2 \rightarrow \dots \rightarrow i_m = l$ such that $\omega_{i_j i_{j+1}} > 0$ for $j = 1, \dots, m - 1$,

which yields $\mathbb{K}_{i_j i_{j+1}}(p) > 0$. This leads to $y_k = y_{i_1} = \dots = y_{i_m} = y_l$. This verifies that $y \in \text{span}(\mathbb{1}_n)$, thus $\text{Ker}(\mathbb{K}(p)) \subset \text{span}(\mathbb{1}_n)$. It is clear that $\text{span}(\mathbb{1}_n) \subset \text{Ker}(\mathbb{K}(p))$ since $\mathbb{K}(p)$ is row-sum-zero and symmetric. Thus we have proved $\text{Ker}(\mathbb{K}(p)) = \text{span}(\mathbb{1}_n)$. \blacksquare

Derivation of $\text{gradD}_f(p|\pi)$: Denote the tangent space of $\mathbb{P}(V)$ at p by $\mathbb{T}_p\mathbb{P}(V)$, and denote the Wasserstein gradient on $(\mathbb{P}(V), g_W)$ by $\text{gradD}_f(p|\pi) \in \mathbb{T}_p\mathbb{P}(V) = \mathbb{1}_n^\perp$. We consider arbitrary curve $\{p(t)\}$ passing through p at $t = 0$, by the definition of the gradient operator on Riemannian manifold (see Lee, 2018, Chapter 2)

$$\left. \frac{d}{dt} \text{D}_f(p_t|\pi) \right|_{t=0} = g_W(\text{gradD}_f(p|\pi), \dot{p}(0)).$$

Denote $\nabla_p \text{D}_f(p|\pi)$ as the flat gradient of f -divergence with respect to p , for any $\dot{p}(0) \in \mathbb{1}_n^\perp$, we have

$$\nabla_p \text{D}_f(p|\pi)(\dot{p}(0))^\top = \text{gradD}_f(p|\pi) \mathbb{K}(p)^\dagger (\dot{p}(0))^\top.$$

Let $\Pi : \mathbb{R}^n \rightarrow \mathbb{R}^n$ be the orthogonal projection onto $\mathbb{T}_p\mathbb{P}(V) = \mathbb{1}_n^\perp$, the above equation yields

$$\Pi(\text{gradD}_f(p|\pi) \mathbb{K}(p)^\dagger) = \Pi(\nabla_p \text{D}_f(p|\pi)).$$

Since $\mathbb{K}(p)^\dagger$ is the Moore-Penrose inverse of $\mathbb{K}(p)$, we have $\Pi = \mathbb{K}(p)^\dagger \mathbb{K}(p) = \mathbb{K}(p) \mathbb{K}(p)^\dagger$. The above equation then leads to

$$(\text{gradD}_f(p|\pi) \mathbb{K}(p)^\dagger) \mathbb{K}(p) \mathbb{K}(p)^\dagger = \nabla_p \text{D}_f(p|\pi) \mathbb{K}(p) \mathbb{K}(p)^\dagger.$$

The left-hand side equals $\text{gradD}_f(p|\pi) \mathbb{K}(p)^\dagger$, as $\text{gradD}_f(p|\pi) \in \mathbb{T}_p\mathbb{P}(V) = \mathbb{1}_n^\perp$. Then,

$$[\text{gradD}_f(p|\pi) - \nabla_p \text{D}_f(p|\pi) \mathbb{K}(p)] \mathbb{K}(p)^\dagger = 0.$$

Furthermore, as

$$\text{Ker}(\mathbb{K}(p)^\dagger) = \text{Ker}(\mathbb{K}(p)) = \text{span}(\mathbb{1}_n),$$

we have

$$\text{gradD}_f(p|\pi) - \nabla_p \text{D}_f(p|\pi) \mathbb{K}(p) \in \text{span}(\mathbb{1}_n).$$

On the other hand, notice that $\text{Ran}(\mathbb{K}(p)) = \text{Ker}(\mathbb{K}(p)^\top)^\perp = \text{Ker}(\mathbb{K}(p))^\perp = \mathbb{1}_n^\perp$, we have $\nabla_p \text{D}_f(p|\pi) \mathbb{K}(p) \in \mathbb{1}_n^\perp$. As a result,

$$\text{gradD}_f(p|\pi) - \nabla_p \text{D}_f(p|\pi) \mathbb{K}(p) \in \text{span}(\mathbb{1}_n) \cap \mathbb{1}_n^\perp = 0.$$

Appendix B. Eigenvalues and eigenvectors of Q -matrix

While the majority of the MCMC literature emphasizes the transition probability matrix P , rather than the transition rate matrix Q , the two are closely related. For completeness, we include a self-contained discussion.

Recall $\omega = (\omega_{ij}) = \text{diag}(\pi)Q$ is a symmetric and row-zero-sum matrix.

Lemma 11 (Sylvester's law of inertia) *Two symmetric square matrices A, B of the same size have the same number of positive, negative and zero eigenvalues if and only if they are congruent, that is, $B = Q A Q^T$ for some non-singular matrix Q .*

Lemma 12 *Given a nondegenerate target distribution π and an irreducible transition rate matrix Q that satisfy the detailed balance condition. Now define $\omega = \text{diag}(\pi)Q$. Then*

- a) ω is a negative semi-definite matrix. Furthermore, $\text{Ker}(\omega) = \text{span}(\mathbb{1}_n)$, and ω is negative definite on $\mathbb{1}_n^\perp$.
- b) The eigenvalues to Q consist of 0 with algebraic multiplicity 1, along with $(n - 1)$ negative eigenvalues.

Proof For part a), follow the same proof technique in Theorem 10, we can show that for arbitrary $x = [x_1, \dots, x_n]$, $x\omega x^\top \leq 0$, as well as $\text{Ker}(\omega) = \text{span}(\mathbb{1}_n)$.

Combining these facts, together with ω being symmetric matrix, it is straightforward to prove that ω is negative definite on $\mathbb{1}_n^\perp$. Since 0 is apparently an eigenvalue to ω with the eigenvector $\mathbb{1}_n$, Recall all eigenvalues to a real symmetric matrix are real, thus ω persists $(n - 1)$ real negative eigenvalues.

For part b), note that

$$Q = \text{diag}(\pi)^{-1}\omega = \sqrt{\text{diag}(\pi)}^{-1}(\sqrt{\text{diag}(\pi)}^{-1}\omega\sqrt{\text{diag}(\pi)}^{-1})\sqrt{\text{diag}(\pi)},$$

Since ω and $(\sqrt{\text{diag}(\pi)}^{-1}\omega\sqrt{\text{diag}(\pi)}^{-1})$ are congruent, by the Sylvester's law of inertia, they have the same number of negative eigenvalues and zero eigenvalue. $(\sqrt{\text{diag}(\pi)}^{-1}\omega\sqrt{\text{diag}(\pi)}^{-1})$ and Q are similar, thus they have the same eigenvalues with the same algebraic multiplicity. In summary, Q has the same number of negative eigenvalues and zero eigenvalue as ω . ■

Alternatively, given an irreducible transition rate matrix Q , we may define $P = I_n + Q\Delta t$ for small enough Δt such that P is an irreducible, aperiodic transition probability matrix. Once applying Perron-Frobenius Theorem onto P and combining the detailed balance, we obtain the same conclusion about Q .

Lemma 13 (Perron-Frobenius Theorem) *Any irreducible, aperiodic transition matrix P has an eigenvalue $\lambda_0 = 1$ with algebraic multiplicity 1 as the Perron-Frobenius eigenvalue, and all other eigenvalues λ_i satisfy $|\lambda_i| < 1$.*

Appendix C. Derivation of our models

C.1 General Jump Process (23)

To construct a sampling algorithm (a “jump process” of particles on V), we rewrite the equation of the state variables p in the form of the forward master equation (3), while leaving the momentum variables ψ as a parameter in the transition rate matrix Q . By splitting the positive part $(\psi_i - \psi_j)_+ := \max\{\psi_i - \psi_j, 0\}$ and the negative part $(\psi_i - \psi_j)_- :=$

– $\min\{\psi_i - \psi_j, 0\}$, recall $(\omega_{ij}), (\theta_{ij}(p))$ are symmetric, we have

$$\begin{aligned}
 & \sum_{j \neq i} \omega_{ij} \theta_{ij}(p) (\psi_i - \psi_j) = \sum_{j \neq i} \omega_{ij} \theta_{ij}(p) [(\psi_i - \psi_j)_+ - (\psi_i - \psi_j)_-] \\
 &= - \sum_{j \neq i} \omega_{ij} \theta_{ij}(p) (\psi_i - \psi_j)_- + \sum_{j \neq i} \omega_{ji} \theta_{ji}(p) (\psi_i - \psi_j)_+ \\
 &= - \left[\sum_{j \neq i} \frac{\omega_{ij} \theta_{ij}(p) (\psi_i - \psi_j)_-}{p_i} \right] p_i + \sum_{j \neq i} \frac{\omega_{ji} \theta_{ji}(p) (\psi_i - \psi_j)_+}{p_j} p_j \\
 &= p \left[\frac{\omega_{1i} \theta_{1i}(p) (\psi_i - \psi_1)_+}{p_1} \dots - \left[\sum_{j \neq i} \frac{\omega_{ij} \theta_{ij}(p) (\psi_i - \psi_j)_-}{p_i} \right] \dots \frac{\omega_{ni} \theta_{ni}(p) (\psi_i - \psi_n)_+}{p_n} \right]^\top
 \end{aligned}$$

This contributes the i -th column of the matrix \bar{Q}_ψ^r in (24). One can easily verify that \bar{Q}_ψ^r is row-sum-zero. On i -th row, if $\psi_i \geq \psi_j$, then $(\psi_j - \psi_i)_+ = 0$ while $(\psi_i - \psi_j)_- = 0$; if $\psi_i \leq \psi_j$, then $(\psi_j - \psi_i)_+ = \psi_j - \psi_i$ while $(\psi_i - \psi_j)_- = \psi_j - \psi_i$. In either cases, the cancellation results in row-sum-zero.

C.2 Chi-squared method

$\theta_{ij} = 1$ and $\mathcal{U}(p) = D_f(p||\pi) = \frac{1}{2} \sum_{i=1}^n \frac{(p_i - \pi_i)^2}{\pi_i}$ are obtained from choosing $f(x) = \frac{1}{2}|x - 1|^2$ in (8) and (6). (26) is obtained from (21) by the direct plug-in.

From (26), we take additional derivative w.r.t t ,

$$\begin{aligned}
 \frac{d^2 p_i}{dt^2} &= \frac{d\psi_i}{dt} \sum_{j \neq i} \omega_{ij} - \sum_{j \neq i} \frac{d\psi_j}{dt} \omega_{ji} \\
 &= -\gamma(t) \left(\psi_i \sum_{j \neq i} \omega_{ij} - \sum_{j \neq i} \psi_j \omega_{ji} \right) - \frac{p_i}{\pi_i} \sum_{j \neq i} \pi_i Q_{ij} + \sum_{j \neq i} \frac{p_j}{\pi_j} \pi_j Q_{ji} + \sum_{j \neq i} \omega_{ij} - \sum_{j \neq i} \omega_{ji} \\
 &= -\gamma(t) \frac{dp_i}{dt} - \sum_{j \neq i} (p_i Q_{ij} - p_j Q_{ji}),
 \end{aligned}$$

where we use $\omega_{ij} = \omega_{ji}$, and obtain the Telegrapher's equation (28).

Denote Δt by the step size, one possible time-discretization for the Telegrapher's equation (28) reads

$$\frac{p_i^{(k+2)} - 2p_i^{(k+1)} + p_i^{(k)}}{(\Delta t)^2} + \gamma(t) \frac{p_i^{(k+1)} - p_i^{(k)}}{\Delta t} = \sum_{j \neq i} (p_j^{(k)} Q_{ji} - p_i^{(k)} Q_{ij}).$$

Thus we obtain

$$p_i^{(k+2)} = p_i^{(k)} + (2 - \gamma(t)\Delta t)(p_i^{(k+1)} - p_i^{(k)}) + (\Delta t)^2 \sum_{j \neq i} (p_j^{(k)} Q_{ji} - p_i^{(k)} Q_{ij}),$$

and note the discretization of (21a) is

$$\begin{aligned} \frac{p_i^{(k+1)} - p_i^{(k)}}{\Delta t} &= \sum_{j \neq i} \omega_{ij} (\psi_i^{(k)} - \psi_j^{(k)}) \\ &= \sum_{j \neq i} \frac{\pi_j Q_{ji} (\psi_i^{(k)} - \psi_j^{(k)})_+}{p_j^{(k)}} p_j^{(k)} + \left[- \sum_{j \neq i} \frac{\pi_i Q_{ij} (\psi_i^{(k)} - \psi_j^{(k)})_-}{p_i^{(k)}} \right] p_i^{(k)}. \end{aligned}$$

Combining both discretizations, the update of the **Chi-squared** method is given by

$$\begin{aligned} p_i^{(k+2)} &= p_i^{(k)} + (\Delta t)^2 \sum_{j \neq i} \left[Q_{ji} + \frac{2 - \gamma(t) \Delta t \pi_j Q_{ji} (\psi_i^{(k)} - \psi_j^{(k)})_+}{\Delta t p_j^{(k)}} \right] p_j^{(k)} \\ &\quad + (\Delta t)^2 \left[-Q_{ij} - \sum_{j \neq i} \frac{\pi_i Q_{ij} (\psi_i^{(k)} - \psi_j^{(k)})_-}{p_i^{(k)}} \right] p_i^{(k)}. \end{aligned}$$

This is a nonlinear jump process from $p_i^{(k)}$ to $p_i^{(k+2)}$. As a comparison, the jump process from MH is

$$p_i^{(k+1)} = p_i^{(k)} + \Delta t \sum_{j \neq i} \left[Q_{ji} p_j^{(k)} - Q_{ij} p_i^{(k)} \right].$$

C.3 KL method

We pick $f(x) = x \log x$ in (8) and (6), which results in $\theta_{ij}(p) = \frac{\frac{p_j}{\pi_j} - \frac{p_i}{\pi_i}}{\log \frac{\pi_i p_j}{\pi_j p_i}}$ and $\mathcal{U}(p) = D_f(p \parallel \pi) = \sum_{i=1}^n p_i \log \frac{p_i}{\pi_i}$. We can compute

$$\frac{\partial \theta_{ij}(p)}{\partial p_i} = \frac{\frac{\log \frac{p_i}{\pi_i} - \log \frac{p_j}{\pi_j}}{\pi_i} - \left(\frac{p_i}{\pi_i} - \frac{p_j}{\pi_j} \right) \frac{\pi_i}{p_i} \frac{1}{\pi_i}}{\left(\log \frac{p_i}{\pi_i} - \log \frac{p_j}{\pi_j} \right)^2} = \frac{\log \left(\frac{\pi_j p_i}{\pi_i p_j} \right) - 1 + \left(\frac{\pi_j p_i}{\pi_i p_j} \right)^{-1}}{\log^2 \left(\frac{\pi_j p_i}{\pi_i p_j} \right)} \frac{1}{\pi_i}.$$

Plugging into (21), we obtain (30).

C.4 log-Fisher method

We still select $f(x) = x \log x$ for $\theta(x, y) = \frac{x-y}{f'(x)-f'(y)}$ just as in KL method, and plug it in the relative Fisher information $I(p \parallel \pi)$

$$I(p \parallel \pi) = \frac{1}{4} \sum_{i,j=1}^n \omega_{ij} \theta_{ij}(p) \left(f' \left(\frac{p_i}{\pi_i} \right) - f' \left(\frac{p_j}{\pi_j} \right) \right)^2 = \frac{1}{4} \sum_{i=1}^n \sum_{j \neq i} \omega_{ij} \left(\log \frac{p_i}{\pi_i} - \log \frac{p_j}{\pi_j} \right) \left(\frac{p_i}{\pi_i} - \frac{p_j}{\pi_j} \right).$$

Note that $\frac{\partial}{\partial p_i} I(p \parallel \pi) = \frac{1}{2\pi_i} \sum_{j \neq i} \omega_{ij} \left[\log \left(\frac{\pi_j p_i}{\pi_i p_j} \right) + 1 - \left(\frac{\pi_j p_i}{\pi_i p_j} \right)^{-1} \right]$. Hence, (21) turns into (31).

Appendix D. Hessian and geodesic convexity

We follow the setting and notations of discussions in Mielke (2013). Consider the space $\mathbb{P}(V)$ of probability measures on a graph $G = (V, E, \omega)$, with the Onsager's response matrix \mathbb{K} defined in (9), let $\{p(t)\}_{t \geq 0}$ be a geodesic on $\mathbb{P}(V)$, then it satisfies the geodesic equations:

$$\begin{cases} \dot{p}(t) = \psi \mathbb{K} \\ \dot{\psi}(t) = -\nabla_p \left(\frac{1}{2} \psi \mathbb{K} \psi^\top \right), \end{cases}$$

Any functional $\mathcal{U}(p)$ that is geodesically λ -strongly convex can be characterized by

$$\frac{d^2}{dt^2} \mathcal{U}(p(t)) \geq \lambda \dot{p}(t) \mathbb{K}^\dagger(p(t)) (\dot{p}(t))^\top.$$

In our case, $\mathbb{K}(p)$ does not depend on p . Here we denote $D^2\mathcal{U}(p)$ as the Hessian of $\mathcal{U}(p)$ in the Euclidean space. The geodesic equation is simplified as

$$\begin{cases} \dot{p}(t) = \psi K \\ \dot{\psi}(t) = 0. \end{cases}$$

Thus $\mathcal{U}(p)$ is geodesically λ -strongly convex if and only if $\dot{p} D^2\mathcal{U}(p) \dot{p}^\top \geq \lambda \dot{p} K^\dagger \dot{p}^\top$, or equivalently, $\psi K D^2\mathcal{U}(p) K^\top \psi^\top \geq \lambda \psi K \psi^\top$. Thus under the flat metric K , we can say $\mathcal{U}(p)$ is geodesically λ -strongly convex, if there exists some $\lambda > 0$, such that for any t , the Rayleigh quotient problem has a lower bound along the dynamics:

$$\lambda \leq \min_{\psi \mathbf{1}_n^\top = 0} \frac{\psi K D^2\mathcal{U}(p(t)) K^\top \psi^\top}{\psi K \psi^\top}.$$

In the **con-Fisher** method, recall $\mathcal{U}(p) = I(p|\pi) = \frac{1}{4} \sum_{i=1}^n \sum_{j \neq i} \omega_{ij} \theta_{ij} (\log \frac{p_i}{\pi_i} - \frac{p_j}{\pi_j})^2$. Thus $\partial_{ii} \mathcal{U}(p) = \sum_{j \neq i} \frac{\omega_{ij} \theta_{ij}}{p_i^2} [1 - \log \left(\frac{\pi_j p_i}{\pi_i p_j} \right)]$ and $\partial_{ij} \mathcal{U}(p) = -\frac{\omega_{ij} \theta_{ij}}{p_i p_j}$, thus the Hessian $D^2\mathcal{U}(p)$ is given by

$$\begin{bmatrix} \sum_{j \neq 1} \frac{\omega_{1j} \theta_{1j}}{p_1^2} [1 - \log \left(\frac{\pi_j p_1}{\pi_1 p_j} \right)] & -\frac{\omega_{12} \theta_{12}}{p_1 p_2} & \dots & -\frac{\omega_{1n} \theta_{1n}}{p_1 p_n} \\ -\frac{\omega_{21} \theta_{21}}{p_2 p_1} & \sum_{j \neq 2} \frac{\omega_{2j} \theta_{2j}}{p_2^2} [1 - \log \left(\frac{\pi_j p_2}{\pi_2 p_j} \right)] & \dots & -\frac{\omega_{2n} \theta_{2n}}{p_2 p_n} \\ \vdots & \dots & \ddots & \vdots \\ -\frac{\omega_{n1} \theta_{n1}}{p_n p_1} & -\frac{\omega_{n2} \theta_{n2}}{p_n p_2} & \dots & \sum_{j \neq n} \frac{\omega_{nj} \theta_{nj}}{p_n^2} [1 - \log \left(\frac{\pi_j p_n}{\pi_n p_j} \right)] \end{bmatrix}.$$

In the asymptotical limit $|\frac{p_i}{\pi_i} - 1| \propto \mathcal{O}(10^{-k})$ for some $k \gg 1$, then

$$\log \frac{\pi_j p_i}{\pi_i p_j} \approx (c_i - c_j) 10^{-k}; \quad \frac{1}{p_i^2} \approx \frac{1}{\pi_i^2} - \frac{2c_i}{p_i^2} 10^{-k}; \quad \text{and} \quad \frac{1}{p_i p_j} \approx \frac{1}{\pi_i \pi_j} - \frac{c_i + c_j}{\pi_i \pi_j} 10^{-k}.$$

Thus the Hessian $D^2\mathcal{U}(p)$ is approximated by

$$\begin{aligned} & \begin{bmatrix} \frac{1}{\pi_1} & 0 & \cdots & 0 \\ 0 & \frac{1}{\pi_2} & \vdots & 0 \\ 0 & 0 & \ddots & 0 \\ 0 & 0 & \cdots & \frac{1}{\pi_n} \end{bmatrix} \begin{bmatrix} \sum_{j \neq 1} \omega_{1j} \theta_{1j} & -\omega_{12} \theta_{12} & \cdots & -\omega_{1n} \theta_{1n} \\ -\omega_{21} \theta_{21} & \sum_{j \neq 2} \omega_{2j} \theta_{2j} & \vdots & -\omega_{2n} \theta_{2n} \\ \vdots & \cdots & \ddots & \vdots \\ -\omega_{n1} \theta_{n1} & \omega_{n2} \theta_{n2} & \cdots & \sum_{j \neq n} \omega_{nj} \theta_{nj} \end{bmatrix} \begin{bmatrix} \frac{1}{\pi_1} & 0 & \cdots & 0 \\ 0 & \frac{1}{\pi_2} & \vdots & 0 \\ 0 & 0 & \ddots & 0 \\ 0 & 0 & \cdots & \frac{1}{\pi_n} \end{bmatrix} \\ & = \text{diag}(\pi^{-1}) K \text{diag}(\pi^{-1}). \end{aligned}$$

Moreover, $D^2\mathcal{U}(p)|_{p=\pi} = \text{diag}(\pi^{-1}) K \text{diag}(\pi^{-1})$.

Let's go back to the Rayleigh quotient problem. As K is symmetric, and $\text{Ker}(K) = \text{span}(\mathbf{1}_n)$, the singular value decomposition (SVD) of K is given by

$$K = U \Sigma U^\top = \widehat{U} \widehat{\Sigma} \widehat{U}^\top.$$

Here $U \in \mathbb{R}^{n \times n}$ is an orthogonal matrix, $\Sigma = \text{diag}(\sigma_1, \dots, \sigma_{n-1}, 0)$ with $\sigma_1 \geq \dots \geq \sigma_{n-1} > 0$, $\widehat{U} \in \mathbb{R}^{n \times (n-1)}$ denotes the matrix formed by the first $n-1$ columns of U , and $\widehat{\Sigma} = \text{diag}(\sigma_1, \dots, \sigma_{n-1})$. Then, we can reformulate the Rayleigh quotient as

$$\min_{\psi \mathbf{1}_n^\top = 0} \frac{\psi \widehat{U} \widehat{\Sigma} \widehat{U}^\top D^2\mathcal{U}(p) \widehat{U} \widehat{\Sigma} \widehat{U}^\top \psi^\top}{\psi \widehat{U} \widehat{\Sigma} \widehat{U}^\top \psi^\top}.$$

Denote $\varphi = \psi \widehat{U} \sqrt{\widehat{\Sigma}}$. As both $\widehat{U} \in \mathbb{R}^{n \times (n-1)}$, $\widehat{\Sigma} \in \mathbb{R}^{(n-1) \times (n-1)}$ are matrices with full rank, $\varphi \in \mathbb{R}^{n-1}$ explores the entire space \mathbb{R}^{n-1} as ψ goes over \mathbb{R}^n . We can further rewrite it as

$$\min_{\varphi \in \mathbb{R}^{n-1}} \frac{\varphi \sqrt{\widehat{\Sigma}} \widehat{U}^\top D^2\mathcal{U}(p) \widehat{U} \sqrt{\widehat{\Sigma}} \varphi^\top}{\varphi \varphi^\top} = \lambda_{\min}(\sqrt{\widehat{\Sigma}} \widehat{U}^\top D^2\mathcal{U}(p) \widehat{U} \sqrt{\widehat{\Sigma}}). \quad (39)$$

Appendix E. Other proofs

Proof [Proof to Lemma 3] Recall

$$\frac{\partial \mathbf{I}(p|\pi)}{\partial p_i} = \frac{1}{2} \sum_{j=1, j \neq i}^n \frac{\omega_{ij}}{\pi_i} (\log \frac{p_i}{\pi_i} - \log \frac{p_j}{\pi_j}) + \frac{\omega_{ij}}{p_i} (\frac{p_i}{\pi_i} - \frac{p_j}{\pi_j}).$$

It is straightforward to verify that when $p = \pi$, we have $\nabla_p \mathbf{I}(p|\pi) = 0$.

On the other hand, suppose $\nabla_p \mathbf{I}(p|\pi) = 0$ and assume $\frac{p_{i_1}}{\pi_{i_1}} \geq \frac{p_j}{\pi_j}$ for any $j \in V$. We will in the end show that $\frac{p_j}{\pi_j} = \frac{p_{i_1}}{\pi_{i_1}}$, thus $p = \pi$ in $\mathbb{P}(V)$.

For any $i \in V$, denote the neighbors of vertex i as $N(i) = \{j \in V \mid \omega_{ij} > 0\}$. Note that

$$0 = \frac{\partial \mathbf{I}(p|\pi)}{\partial p_{i_1}} = \frac{1}{2} \sum_{j \in N(i_1)} \frac{\omega_{i_1 j}}{\pi_{i_1}} (\log \frac{p_{i_1}}{\pi_{i_1}} - \log \frac{p_j}{\pi_j}) + \frac{\omega_{i_1 j}}{p_{i_1}} (\frac{p_{i_1}}{\pi_{i_1}} - \frac{p_j}{\pi_j}) \geq 0,$$

as $\frac{p_{i_1}}{\pi_{i_1}} \geq \frac{p_j}{\pi_j}$ and $\omega_{i_1 j} > 0$. This implies that for any $j \in N(i_1)$, $\frac{p_j}{\pi_j} = \frac{p_{i_1}}{\pi_{i_1}}$.

As the graph $G = (V, E, \omega)$ is connected, for any node j , there exists a path $i_1 \rightarrow i_2 \rightarrow \dots \rightarrow i_m = j$ for some $m \leq n$, such that $\omega_{i_k i_{k+1}} > 0$ for $k = 1, \dots, m-1$. From the

previous step, we have shown that $i_2 \in N(i_1)$ implies that $\frac{p_{i_2}}{\pi_{i_2}} = \frac{p_{i_1}}{\pi_{i_1}}$. Thus we can repeat this process for i_2, \dots, i_m , and prove that

$$\frac{p_{i_1}}{\pi_{i_1}} = \frac{p_{i_2}}{\pi_{i_2}} = \dots = \frac{p_j}{\pi_j}.$$

In conclusion, we have shown that $\frac{p_j}{\pi_j} = \frac{p_{i_1}}{\pi_{i_1}}$ for all $j \in V$. Since p is a probability function and must sum to one, it follows that $p = \pi$. ■

Proof [Proof of Theorem 4] Fix r_0 , $F_{r_0}(r)$ is invertible on $(0, r_0]$, and we denote its inverse by $F_{r_0}^{-1}(C)$, whose domain is $[0, \infty)$ and range is $(0, r_0]$. Note that for $r \in (0, r_0]$ and $C \in (0, \infty)$,

$$F_{r_0}(r) \leq C, \quad \text{if and only if} \quad F_{r_0}^{-1}(C) \leq r. \quad (40)$$

Pick $C \in (0, \infty)$. Let us suppose $F_{r_0}^{-1}(C) = r$ for some $r \in (0, r_0]$, that is $F_{r_0}(r) = C$. For any $r_1 > r_0$, $F_{r_1}(r) > F_{r_0}(r) = C$ implies that $F_{r_1}^{-1}(C) > r = F_{r_0}^{-1}(C)$. Now for fixed C , define $G_C(r) = F_r^{-1}(C)$, thus $G_C(r)$ is a strictly increasing function, satisfying that $G_C(r) > 0$ as long as $C > 0$ and $r > 0$. And

$$G_C(r_0) = F_{r_0}^{-1}(C) \leq r, \quad \text{if and only if} \quad F_{r_0}(r) \leq C. \quad (41)$$

Given that the Hamiltonian $\mathcal{H}(p(t), \psi(t))$ is nonincreasing as shown in (22), and $\mathcal{H}(p(0), \psi(0))$ is bounded, let $r_i = \frac{p_i}{\pi_i}$, for any t ,

$$\mathcal{U}(p(t)) = \frac{1}{4} \sum_{i,j=1}^n F_{r_i}(r_j) \omega_{ij} \leq \mathcal{H}(p(t), \psi(t)) \leq C,$$

which implies that $F_{r_i}(r_j) \omega_{ij} \leq C$ for any pair (i, j) .

Assume $r_{i_1} \geq r_i$ for any $i \in V$. Note that there exists an index i such that $p_i \geq \frac{1}{n}$. Then

$$r_{i_1} = \max r_i \geq r_i = \frac{p_i}{\pi_i} \geq \frac{1}{n\pi_i} \geq \frac{1}{n \max \pi_i} > 0.$$

Since the graph G is connected, for any node j , there exists a path $i_1 \rightarrow i_2 \rightarrow \dots \rightarrow i_m = j$ for some $m \leq n$, such that $\omega_{i_k i_{k+1}} > 0$ for $k = 1, \dots, m-1$. Let $\bar{\omega} = \min_k \omega_{i_k i_{k+1}} > 0$. For $k = 1, \dots, m-1$, $F_{r_{i_k}}(r_{i_{k+1}}) \omega_{i_k i_{k+1}} \leq C$ implies that $F_{r_{i_k}}(r_{i_{k+1}}) \leq \frac{C}{\omega_{i_k i_{k+1}}} \leq \frac{C}{\bar{\omega}}$.

From node i_1 to i_2 , given that $r_{i_1} \geq r_{i_2}$ and $F_{r_{i_1}}(r_{i_2}) \leq \frac{C}{\bar{\omega}}$, by (40), (41) and $G_C(r)$ is strictly increasing, we have

$$r_{i_2} \geq F_{r_{i_1}}^{-1}\left(\frac{C}{\bar{\omega}}\right) = G_{C/\bar{\omega}}(r_{i_1}) \geq G_{C/\bar{\omega}}\left(\frac{1}{n \max \pi_i}\right) > 0.$$

From node i_2 to i_3 , if $r_{i_2} \geq r_{i_3}$, we can repeat the above step and yield $r_{i_3} \geq G_{C/\bar{\omega}}(r_{i_2})$; otherwise $r_{i_3} > r_{i_2} \geq G_{C/\bar{\omega}}(r_{i_1}) \geq G_{C/\bar{\omega}}(r_{i_2})$. In either case,

$$r_{i_3} \geq G_{C/\bar{\omega}}(r_{i_2}) \geq G_{C/\bar{\omega}}(G_{C/\bar{\omega}}(r_{i_1})) \geq G_{C/\bar{\omega}}^{(2)}\left(\frac{1}{n \max \pi_i}\right) > 0.$$

We may repeat this argument and yield that $r_{i_k} > 0$ for any node i_k on this path,

$$r_{i_k} \geq G_{C/\bar{\omega}}^{(k-1)}\left(\frac{1}{n \max \pi_i}\right) > 0.$$

Thus $\varepsilon = (\min \pi_i) \cdot G_{C/\bar{\omega}}^{(n-1)}\left(\frac{1}{n \max \pi_i}\right) > 0$ is the lower bound of $p_i(t)$. ■

Proof [Proof to Lemma 9] Follow the notations used in Appendix D, Recall (39) and

$$D^2\mathcal{U}(p)|_{p=\pi} = \text{diag}(\pi^{-1})K\text{diag}(\pi^{-1}) = \text{diag}(\pi)^{-1}\widehat{U}\widehat{\Sigma}\widehat{U}^\top\text{diag}(\pi)^{-1}.$$

The minimal positive eigenvalue λ at $p = \pi$ is

$$\begin{aligned} \lambda &= \lambda_{\min}\left(\underbrace{\sqrt{\widehat{\Sigma}}\widehat{U}^\top\text{diag}(\pi)^{-1}\widehat{U}\widehat{\Sigma}}_S \underbrace{\widehat{U}^\top\text{diag}(\pi)^{-1}\widehat{U}}_{S^\top} \sqrt{\widehat{\Sigma}}\right) \\ &= \lambda_{\min}\left((S^\top\sqrt{\widehat{\Sigma}})^\top\widehat{\Sigma}(S^\top\sqrt{\widehat{\Sigma}})\right). \end{aligned}$$

Since the non-singular conjugate of positive definite matrix is still positive definite, we can show that $\lambda > 0$ as long as $S^\top\sqrt{\widehat{\Sigma}}$ is non-singular.

In fact, suppose for $x \in \mathbb{R}^{n-1}$, $S^\top\sqrt{\widehat{\Sigma}}x^\top = 0$, thus $(\sqrt{\widehat{\Sigma}}x^\top)^\top S^\top\sqrt{\widehat{\Sigma}}x^\top = 0$. From the change of variable $y^\top = \widehat{U}\sqrt{\widehat{\Sigma}}x^\top \in \mathbb{R}^n$, we obtain $y\text{diag}(\pi)^{-1}y^\top = 0$. This leads to $y = 0$, i.e., $\widehat{U}\sqrt{\widehat{\Sigma}}x^\top = 0$. Now since $\widehat{U} \in \mathbb{R}^{n \times (n-1)}$ is full rank, $\sqrt{\widehat{\Sigma}}$ is non-singular, we have $x = 0$. As a result, $S^\top\sqrt{\widehat{\Sigma}}$ is non-singular. ■

Appendix F. More numerical results

In this section, we report heuristic observations on sampling behavior generated by the `log-Fisher` method. We use the ‘rose’ dataset discretized on a larger lattice of 100×100 nodes. The target distribution is constructed by assigning mass $p_i \in \{\frac{1}{10}, 1\}$ to each node: larger masses are placed on the support of the ‘rose’, while smaller masses are assigned to the remaining nodes for the background. The target distribution is constructed to be strict positive. Parameters are set as:

$$\text{sampling size } M = 10^6, \quad \text{default step size } \Delta t = 0.1 \quad \text{total iterations } N = 3 \times 10^4.$$

We again employ a constant damping parameter $\gamma(t) = 2\sqrt{\lambda_*}$. Owing to the large state space (10^4 nodes) and the multi-chain nature of our proposed jump process, these experiments are carried out on the UCSB computing cluster. A notable qualitative difference between the `log-Fisher` method and MH sampling is observed in Figure 9: throughout the jump process, the empirical distributions produced by the `log-Fisher` method appear significantly smoother, whereas those generated by MH exhibit a mosaic effect. We conjecture that this behavior is related to the acceptance–rejection matrix (25) inherent in the

log-Fisher method,

$$(\bar{A}_\psi)_{ij} = \max \left\{ \frac{1 - \frac{\pi_i p_j}{\pi_j p_i}}{\log \left(\frac{\pi_j p_i}{\pi_i p_j} \right)} (\psi_j - \psi_i), 0 \right\} A_{ij},$$

which compares the local ratios $\frac{p_i}{\pi_i}$ and $\frac{p_j}{\pi_j}$ across neighboring nodes along edges.

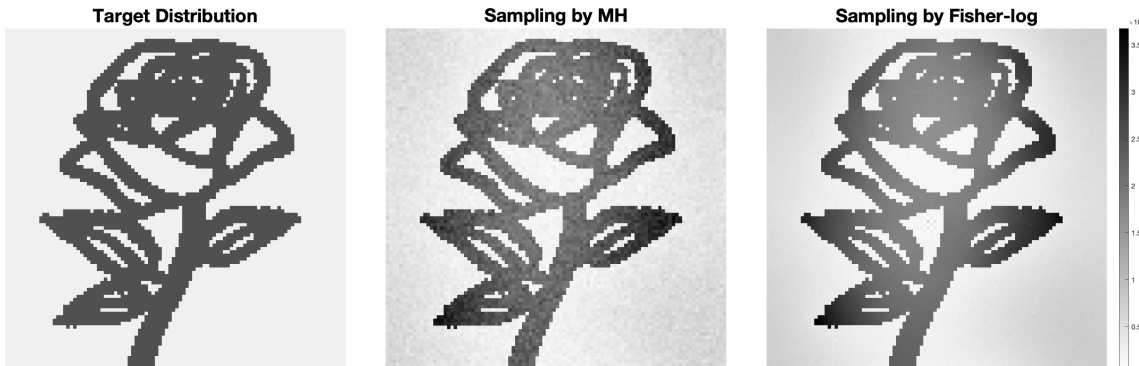


Figure 9: Sampling on a 100×100 lattice graph for the input grayscale image ‘rose’. The target distribution is set to be a piecewise-constant function. Across all simulations, the empirical distributions produced by MH appear less structured than those obtained with the log-Fisher method.

References

- D. Albritton, S. Armstrong, J.-C. Mourrat, and M. Novack. Variational methods for the kinetic Fokker-Planck equation. *Anal. PDE*, 17(6):1953–2010, 2024. ISSN 2157-5045,1948-206X. doi: 10.2140/apde.2024.17.1953.
- F. Alimisis, A. Orvieto, G. Bécigneul, and A. Lucchi. A continuous-time perspective for modeling acceleration in Riemannian optimization. In *International Conference on Artificial Intelligence and Statistics*, pages 1297–1307. PMLR, 2020.
- L. Ambrosio, N. Gigli, and G. Savaré. *Gradient flows in metric spaces and in the space of probability measures*. Lectures in Mathematics ETH Zürich. Birkhäuser Verlag, Basel, second edition, 2008. ISBN 978-3-7643-8721-1.
- A. J. Archer. Dynamical density functional theory for molecular and colloidal fluids: A microscopic approach to fluid mechanics. *The Journal of Chemical Physics*, 130(1):014509, 01 2009. ISSN 0021-9606. doi: 10.1063/1.3054633.
- J.-D. Benamou and Y. Brenier. A computational fluid mechanics solution to the Monge-Kantorovich mass transfer problem. *Numer. Math.*, 84(3):375–393, 2000. ISSN 0029-599X,0945-3245. doi: 10.1007/s002110050002.

- G. Brigati, G. Stoltz, A. Q. Wang, and L. Wang. Explicit convergence rates of underdamped Langevin dynamics under weighted and weak Poincaré–Lions inequalities, 2025. URL <https://arxiv.org/abs/2407.16033>.
- B. Calderhead. A general construction for parallelizing metropolis-hastings algorithms. Proceedings of the National Academy of Sciences, 111(49):17408–17413, 2014. doi: 10.1073/pnas.1408184111.
- Y. Cao, J. Lu, and L. Wang. On explicit L^2 -convergence rate estimate for underdamped Langevin dynamics. Arch. Ration. Mech. Anal., 247(5):Paper No. 90, 34, 2023. ISSN 0003-9527,1432-0673. doi: 10.1007/s00205-023-01922-4.
- S. Chen, Q. Li, O. Tse, and S. J. Wright. Accelerating optimization over the space of probability measures. Journal of Machine Learning Research, 26(31):1–40, 2025. URL <http://jmlr.org/papers/v26/23-1288.html>.
- X. Cheng, N. S. Chatterji, P. L. Bartlett, and M. I. Jordan. Underdamped Langevin MCMC: A non-asymptotic analysis. In Proceedings of the 31st Conference On Learning Theory, volume 75 of Proceedings of Machine Learning Research, pages 300–323, 2018. URL <https://proceedings.mlr.press/v75/cheng18a.html>.
- S.-N. Chow, W. Huang, Y. Li, and H. Zhou. Fokker-Planck equations for a free energy functional or Markov process on a graph. Arch. Ration. Mech. Anal., 203(3):969–1008, 2012. ISSN 0003-9527,1432-0673. doi: 10.1007/s00205-011-0471-6.
- S.-N. Chow, W. Li, and H. Zhou. A discrete Schrödinger equation via optimal transport on graphs. J. Funct. Anal., 276(8):2440–2469, 2019. ISSN 0022-1236,1096-0783. doi: 10.1016/j.jfa.2019.02.005.
- R. V. Craiu, J. Rosenthal, and C. Yang. Learn from thy neighbor: Parallel-chain and regional adaptive mcmc. Journal of the American Statistical Association, 104(488):1454–1466, 2009. doi: 10.1198/jasa.2009.tm08393.
- M. Erbar and J. Maas. Ricci curvature of finite Markov chains via convexity of the entropy. Arch. Ration. Mech. Anal., 206(3):997–1038, 2012. ISSN 0003-9527,1432-0673. doi: 10.1007/s00205-012-0554-z.
- Y. Gao, J.-G. Liu, and W. Li. Master equations for finite state mean field games with nonlinear activations. Discrete Contin. Dyn. Syst. Ser. B, 29(7):2837–2879, 2024. ISSN 1531-3492,1553-524X. doi: 10.3934/dcdsb.2023204.
- A. Gelman and D. B. Rubin. Inference from Iterative Simulation Using Multiple Sequences. Statistical Science, 7(4):457 – 472, 1992. doi: 10.1214/ss/1177011136.
- C. J. Geyer. Introduction to Markov chain Monte Carlo. In Handbook of Markov chain Monte Carlo, Chapman & Hall/CRC Handb. Mod. Stat. Methods, pages 3–48. CRC Press, Boca Raton, FL, 2011. ISBN 978-1-4200-7941-8.
- W. K. Hastings. Monte Carlo sampling methods using Markov chains and their applications. Biometrika, 57(1):97–109, 1970. ISSN 0006-3444,1464-3510. doi: 10.1093/biomet/57.1.97.

- G. E. Hinton, S. Osindero, and Y.-W. Teh. A fast learning algorithm for deep belief nets. Neural Comput., 18(7):1527–1554, 2006. ISSN 0899-7667,1530-888X. doi: 10.1162/neco.2006.18.7.1527.
- P. Jäckel. Monte Carlo methods in finance. John Wiley & Sons, 2002.
- P. Jacob, C. P. Robert, and M. H. Smith. Using parallel computation to improve independent metropolis–hastings based estimation. Journal of Computational and Graphical Statistics, 20(3):616–635, 2011. doi: 10.1198/jcgs.2011.10167.
- E. Jacquier, N. G. Polson, and P. E. Rossi. Bayesian analysis of stochastic volatility models with fat-tails and correlated errors. J. Econometrics, 122(1):185–212, 2004. ISSN 0304-4076,1872-6895. doi: 10.1016/j.jeconom.2003.09.001.
- A. Jasra, D. A. Stephens, and C. C. Holmes. Population-based reversible jump Markov chain Monte Carlo. Biometrika, 94(4):787–807, 2007. ISSN 0006-3444,1464-3510. doi: 10.1093/biomet/asm069.
- M. Jerrum and A. Sinclair. The Markov chain Monte Carlo method: an approach to approximate counting and integration. In Approximation Algorithms for NP-Hard Problems, page 482–520. PWS Publishing Co., 1996. ISBN 0534949681.
- M. I. Jordan, Z. Ghahramani, T. S. Jaakkola, and L. K. Saul. An introduction to variational methods for graphical models. In Learning in Graphical Models, page 105–161. MIT Press, Cambridge, MA, USA, 1999. ISBN 0262600323.
- I. Karatzas, J. Maas, and W. Schachermayer. Trajectoryal dissipation and gradient flow for the relative entropy in Markov chains. Commun. Inf. Syst., 21(4):481–536, 2021. ISSN 1526-7555,2163-4548. doi: 10.4310/CIS.2021.v21.n4.a1.
- S. G. Kou and H. Wang. Option Pricing under a Double Exponential Jump Diffusion Model. Management Science, 50(9):1178–1192, 2004. ISSN 00251909, 15265501. URL <http://www.jstor.org/stable/30046226>.
- D. P. Landau and K. Binder. A guide to Monte Carlo simulations in statistical physics. Cambridge University Press, Cambridge, fourth edition, 2015. ISBN 978-1-107-07402-6. doi: 10.1017/CBO9781139696463.
- N.-T. Le and L. Miclo. Swarm dynamics for global optimization on finite sets. Stochastic Processes and their Applications, 191:104780, 2026. ISSN 0304-4149. doi: <https://doi.org/10.1016/j.spa.2025.104780>.
- J. M. Lee. Introduction to Riemannian manifolds, volume 176 of Graduate Texts in Mathematics. Springer, Cham, second edition, 2018. ISBN 978-3-319-91754-2; 978-3-319-91755-9.
- D. A. Levin, Y. Peres, and E. L. Wilmer. Markov chains and mixing times. American Mathematical Society, Providence, RI, 2009. ISBN 978-0-8218-4739-8. doi: 10.1090/mbk/058.

- R. Li, H. Zha, and M. Tao. Hessian-Free High-Resolution Nesterov Acceleration For Sampling. In Proceedings of the 39th International Conference on Machine Learning, volume 162 of Proceedings of Machine Learning Research, pages 13125–13162, 2022. URL <https://proceedings.mlr.press/v162/li22z.html>.
- W. Li. Geometric calculations on probability manifolds from reciprocal relations in Master equations, 2025. URL <https://arxiv.org/abs/2504.19368>.
- A. Lou, C. Meng, and S. Ermon. Discrete Diffusion Modeling by Estimating the Ratios of the Data Distribution, 2024. URL <https://arxiv.org/abs/2310.16834>.
- Y.-A. Ma, E. B. Fox, T. Chen, and L. Wu. Irreversible samplers from jump and continuous Markov processes. Stat. Comput., 29(1):177–202, 2019. ISSN 0960-3174,1573-1375. doi: 10.1007/s11222-018-9802-x.
- Y.-A. Ma, N. S. Chatterji, X. Cheng, N. Flammarion, P. L. Bartlett, and M. I. Jordan. Is there an analog of Nesterov acceleration for gradient-based MCMC? Bernoulli, 27(3): 1942 – 1992, 2021. doi: 10.3150/20-BEJ1297.
- J. Maas. Gradient flows of the entropy for finite Markov chains. J. Funct. Anal., 261(8): 2250–2292, 2011. ISSN 0022-1236,1096-0783. doi: 10.1016/j.jfa.2011.06.009.
- C. J. Maddison, D. Paulin, Y. W. Teh, B. O’Donoghue, and A. Doucet. Hamiltonian Descent Methods, 2018. URL <https://arxiv.org/abs/1809.05042>.
- S. Majee, A. Abhishek, T. Strauss, and T. Khan. Mcmc-net: accelerating markov chain monte carlo with neural networks for inverse problems. Inverse Problems, 41(9):095013, sep 2025. doi: 10.1088/1361-6420/ae05c2.
- K. L. Mengersen and R. L. Tweedie. Rates of convergence of the Hastings and Metropolis algorithms. Ann. Statist., 24(1):101–121, 1996. ISSN 0090-5364,2168-8966. doi: 10.1214/aos/1033066201.
- N. Metropolis, A. W. Rosenbluth, M. N. Rosenbluth, A. H. Teller, and E. Teller. Equation of State Calculations by Fast Computing Machines. The Journal of Chemical Physics, 21(6):1087–1092, 06 1953. ISSN 0021-9606. doi: 10.1063/1.1699114.
- A. Mielke. Geodesic convexity of the relative entropy in reversible Markov chains. Calc. Var. Partial Differential Equations, 48(1-2):1–31, 2013. ISSN 0944-2669,1432-0835. doi: 10.1007/s00526-012-0538-8.
- R. M. Neal. MCMC using Hamiltonian dynamics. In Handbook of Markov chain Monte Carlo, Chapman & Hall/CRC Handb. Mod. Stat. Methods, pages 113–162. CRC Press, Boca Raton, FL, 2011. ISBN 978-1-4200-7941-8.
- E. Nelson. Derivation of the schrödinger equation from newtonian mechanics. Phys. Rev., 150:1079–1085, Oct 1966. doi: 10.1103/PhysRev.150.1079. URL <https://link.aps.org/doi/10.1103/PhysRev.150.1079>.

- Y. Nesterov. Introductory lectures on convex optimization: A basic course, volume 87 of Applied Optimization. Kluwer Academic Publishers, Boston, MA, 2004. ISBN 1-4020-7553-7. doi: 10.1007/978-1-4419-8853-9.
- Y. E. Nesterov. A method for solving the convex programming problem with convergence rate $O(1/k^2)$. Dokl. Akad. Nauk SSSR, 269(no. 3.):543–547, 1983. ISSN 0002-3264.
- F. Otto. The geometry of dissipative evolution equations: the porous medium equation. Comm. Partial Differential Equations, 26(1-2):101–174, 2001. ISSN 0360-5302,1532-4133. doi: 10.1081/PDE-100002243.
- M. Ottobre. Markov chain Monte Carlo and irreversibility. Rep. Math. Phys., 77(3):267–292, 2016. ISSN 0034-4877,1879-0674. doi: 10.1016/S0034-4877(16)30031-3.
- C. P. Robert and G. Casella. Monte Carlo statistical methods. Springer Texts in Statistics. Springer-Verlag, New York, second edition, 2004. ISBN 0-387-21239-6. doi: 10.1007/978-1-4757-4145-2.
- G. O. Roberts and R. L. Tweedie. Geometric convergence and central limit theorems for multidimensional Hastings and Metropolis algorithms. Biometrika, 83(1):95–110, 1996a. ISSN 0006-3444. doi: 10.1093/biomet/83.1.95.
- G. O. Roberts and R. L. Tweedie. Exponential convergence of Langevin distributions and their discrete approximations. Bernoulli, 2(4):341–363, 1996b. ISSN 1350-7265. doi: 10.2307/3318418.
- R. Salakhutdinov and G. Hinton. Deep Boltzmann Machines. In Proceedings of the Twelfth International Conference on Artificial Intelligence and Statistics, volume 5 of Proceedings of Machine Learning Research, pages 448–455, 2009. URL <https://proceedings.mlr.press/v5/salakhutdinov09a.html>.
- J. Schnakenberg. Network theory of microscopic and macroscopic behavior of master equation systems. Rev. Modern Phys., 48(4):571–585, 1976. ISSN 0034-6861,1539-0756. doi: 10.1103/RevModPhys.48.571.
- W. Su, S. Boyd, and E. J. Candès. A Differential Equation for Modeling Nesterov’s Accelerated Gradient Method: Theory and Insights. Journal of Machine Learning Research, 17(153):1–43, 2016. URL <http://jmlr.org/papers/v17/15-084.html>.
- A. Taghvaei and P. Mehta. Accelerated Flow for Probability Distributions. In Proceedings of the 36th International Conference on Machine Learning, volume 97 of Proceedings of Machine Learning Research, pages 6076–6085, 2019. URL <https://proceedings.mlr.press/v97/taghvaei19a.html>.
- Y. W. Teh, M. Welling, S. Osindero, and G. E. Hinton. Energy-based models for sparse overcomplete representations. Journal of Machine Learning Research, 4(7-8):1235–1260, 2004. ISSN 1532-4435,1533-7928. doi: 10.1162/jmlr.2003.4.7-8.1235.
- C. Villani. Optimal transport: Old and new, volume 338. Springer-Verlag, Berlin, 2009. ISBN 978-3-540-71049-3. doi: 10.1007/978-3-540-71050-9.

- M.-K. von Renesse. An optimal transport view of Schrödinger’s equation. Canad. Math. Bull., 55(4):858–869, 2012. ISSN 0008-4395,1496-4287. doi: 10.4153/CMB-2011-121-9.
- Y. Wang and W. Li. Accelerated information gradient flow. J. Sci. Comput., 90(1):Paper No. 11, 47, 2022. ISSN 0885-7474,1573-7691. doi: 10.1007/s10915-021-01709-3.
- A. Wibisono. Sampling as optimization in the space of measures: The Langevin dynamics as a composite optimization problem. In Proceedings of the 31st Conference On Learning Theory, volume 75 of Proceedings of Machine Learning Research, pages 2093–3027, 2018. URL <https://proceedings.mlr.press/v75/wibisono18a.html>.
- C. Xu, X. Cheng, and Y. Xie. Normalizing flow neural networks by jko scheme. In A. Oh, T. Naumann, A. Globerson, K. Saenko, M. Hardt, and S. Levine, editors, Advances in Neural Information Processing Systems, volume 36, pages 47379–47405. Curran Associates, Inc., 2023. URL https://proceedings.neurips.cc/paper_files/paper/2023/file/93fce71def4e3cf418918805455d436f-Paper-Conference.pdf.
- H. Zhang and S. Sra. Towards Riemannian Accelerated Gradient Methods, 2018. URL <https://arxiv.org/abs/1806.02812>.
- X. Zuo, S. Osher, and W. Li. Gradient-adjusted underdamped langevin dynamics for sampling. SIAM/ASA Journal on Uncertainty Quantification, 13(4):1735–1765, 2025. doi: 10.1137/24M1702015.